Volume 17, Issue 3, 172524 (1-18)

Iranian Journal of Earth Science (IJES)

https://doi.org/10.57647/j.ijes.2025.16794

Geochemistry of core sediments in the southern coast of Caspian Sea, Mazandaran, Iran: Implication for paleoclimate

Afsaneh Dehghan Chenari[1], Sadat Feiznia[2,*], Mohsen Aleali[1], Manouchehr Ghorashi[3]

[1]*Department of Geology, Faculty of Sciences, Science and Research Branch, Islamic Azad University, Tehran, Iran.*
[2]*Department of Reclamation of Arid and Mountainous Regions, Faculty of Natural Resources, University of Tehran, Karaj, Iran.*
[3]*Department of Geology, Faculty of Science, North Tehran Branch, Islamic Azad University, Tehran, Iran.*

[*]**Corresponding author:** sfeiz@ut.ac.ir

Original Research

Received:
9 February 2024
Revised:
10 April 2024
Accepted:
8 June 2024
Published online:
10 July 2025

Abstract:

The present study conducted a geochemical analysis of the core sediments from the Jouybar and Zaghmarz areas located on the South Coast of the Caspian Sea in northern Iran. The aim of the study was to investigate the paleoclimate conditions and recycling effects of these sediments. The cores, named AZS (Azad University Shorsahra area) and AM (Amirabad), have depths of 9.3 m and 8.2 m, respectively. They consist of three lithological units, including sandy mud, mud, and silty sand. A total of 50 samples were collected from these units for X-ray diffraction (XRD), geochemistry (ICP-AES), and radiocarbon analyses.

The X-ray diffraction analysis revealed that the samples predominantly composed of clay and non-clay minerals (e.g., Quartz, Feldspar, and Calcite). Various chemical indexes based on major and trace elements were used to assess the intensity of weathering. The results showed that sandy mud and muddy sediments experienced slightly higher weathering compared to silty sand sediments, indicating a weak to moderate degree of chemical weathering in the source region. Additionally, the A-CN-K and SiO_2 vs. (Al_2O_3+K_2O+Na_2O) plots supported the conclusion of weak to moderate chemical weathering in arid and semi-arid paleoclimate conditions.

Furthermore, the index of compositional variability (ICV) and the relationships between Zr/Sc and Th/Sc ratios suggested that sedimentary recycling in the core sediments was negligible. Binary plots of V/Cr vs. U/Th and Ni/Co vs. U/Th indicated that dysoxic/oxic conditions predominantly prevailed during the deposition of the two cores' sediments.

Keywords: Paleoclimate; Source-area weathering; Core sediments; Caspian Sea; Iran

1. Introduction

The geochemical composition of terrigenous sedimentary rocks is influenced by various factors, including the original composition of rocks in the source area, the degree of chemical weathering, transportation processes, and paleoclimatic conditions (Nesbitt and Young, 1982; Verma and Armstrong-Altrin, 2013; Madhava Raju et al., 2016; Mazumder, 2017). Fine-grained clastic sediments, such as mudstone and claystone, are particularly useful for preserving the geochemical characteristics of the source rocks (Taylor and McLennan, 1985; Cullers, 1988, 2000; Cullers and Podkovyrov, 2000; Hessler and Lowe, 2006; Fu et al., 2011; Wang et al., 2017).

Geochemical investigations of the fine-grained clastic sediments can provide information regarding the degree of chemical weathering of the source material, paleoclimatic conditions, and paleo-redox conditions that existed during their sedimentation. (Selvaraj and Chen, 2006; Gallala et al., 2009; Nesbitt and Young, 1984; McLennan et al., 1993; Cox et al., 1995; Zhang et al., 1998; Jin et al., 2006; Lee, 2009; Al-Khirbash et al., 2013; Sahoo et al., 2016; Christopher and Elderfield, 1990; Jones and Manning, 1994; Nath et al., 1997; Madhava Raju et al., 2016).

The values of the geochemical proxies can indicate both the degree of chemical weathering in the sediments and the conditions of climate evolution (Li et al., 2009). Some trace elements (e.g., Co, Cr, Hf, Sc, Th, and Zr) in the sediments are used to study the source area due to their immobile nature (McLennan et al., 1983; Bhatia and Crook, 1986; Von Eynatten et al., 2003; Tao et al., 2014; Moradi et al., 2016).

Most developed dating techniques, such as AMS14C, OSL, 137Cs, and 210Pb, have been utilized in Holocene paleoclimate reconstruction. Among these methods, AMS14C and OSL are the most widely employed (**Hao2015?**; Gosse and Fred, 2001).

The core sedimentary successions in the Jouybar and Zaghmarz areas, located on the southern coast of the Caspian Sea, are characterized by sandy mud, muddy, and silty sand facies. This study aims to gather information about the history of chemical weathering, the impact of weathering on source rocks, and the conditions of paleo-oxidation and reduction. In this study, an attempt has been made to investigate the geochemical characteristics of the fine-grained sediments from the AZS and AM cores in the Jouybar and Zaghmarz areas due to the absence or lack of information regarding paleoclimate changes and the paleo-oxidation and reduction environment in the middle to late Holocene on the southern coast of the Caspian Sea.

2. Geological setting and lithostratigraphy

The sediment cores AZS (36° 43′ 28.2″ N, 52° 51′ 20.9″ E) and AM (36° 49′ 47.8″ N, 53° 21′ 26.9″ E) were obtained from the southern Iranian part of the Caspian Sea's coastal plain (Fig. 1). The south part of the Jouybar and Zaghmarz areas is characterized by the presence of the Alborz Mountain ridge, known as the Central Alborz Structural Zone (Fig. 1).

The Alborz range began forming in the mid-Cenozoic era due to the uplift resulting from the convergence between the Arabian and Eurasian plates (Aghanabati, 2004). This mountain range contributes a significant amount of clastic material to the southern basin of the Caspian Sea. The geological formations found in the southern part of the Caspian coastal plain include sedimentary rocks (shale, sandstone, marl, and massive limestones), volcanic rocks (basaltic and andesitic), and metamorphic rocks (Aghanabati, 2004; Lahijani and Tavakoli, 2012).

Based on the lithologic characteristics and grain size analysis, the AZS and AM cores have been divided into three lithofacies (Tables 1 and 2). These lithofacies include sandy mud, mud, and silty sand facies (Figs. 2 and 3). The sandy mud facies, with a thickness ranging from 75 to 420 cm, have the maximum thickness in both the AZS and AM cores (Fig. 2).

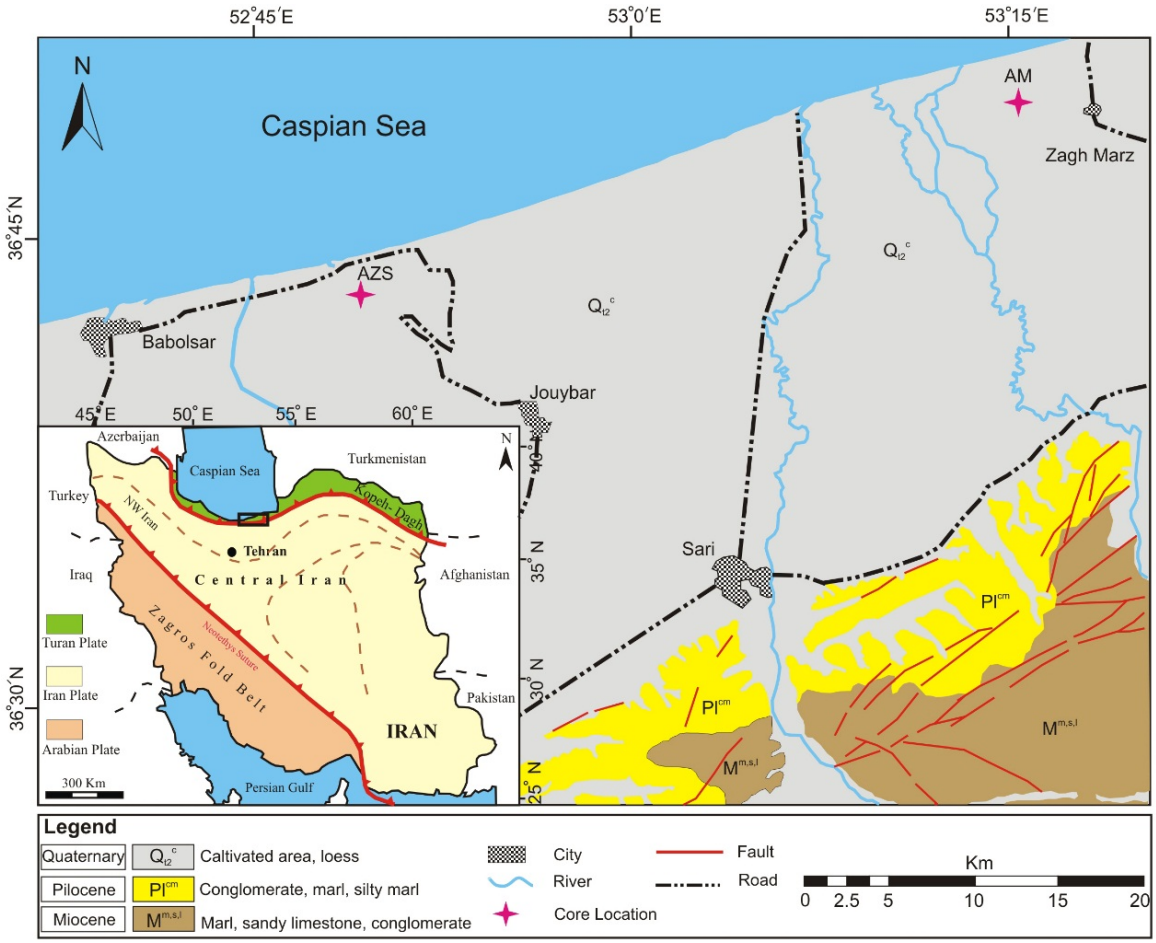

Figure 1. Map of Iran (changed from (Wilmsen et al., 2009)) and the simplified geological map of the south coast of the Caspian Sea (Vahdati Daneshmand and Saidi, 1991) with the location of the two studied cores.

Table 1. Results obtained from grain size analysis of the AZS core sediments.

Sample No.	Depth (cm)	Facies	Clay (%)	Silt (%)	Mud (%)	Sand (%)	Gravel (%)	Sorting
AZS1	20	sandy mud	36.51	45.39	81.90	18.10	0	2.29
AZS2	35	sandy mud	24.55	37.11	61.66	38.30	0	3.07
AZS3	60	sandy mud	28.64	34.33	62.97	37.03	0	3.02
AZS4	155	mud	50.57	39.66	90.23	6.76	0	1.67
AZS5	235	slightly gravelly muddy sand	11.22	16.27	27.49	69.36	3.14	2.59
AZS6	290	sandy mud	42.05	25.34	67.39	32.60	0	2.93
AZS7	310	sandy mud	39.02	43.77	82.79	17.20	0	2.66
AZS8	390	sandy mud	44.85	32.50	77.35	22.70	0	2.61
AZS9	410	sandy mud	29.93	36.82	66.75	33.30	0	2.87
AZS10	470	sandy mud	20.16	49.86	70.02	29.98	0	2.40
AZS11	530	sandy mud	28.91	31.24	60.15	39.90	0	3.13
AZS12	570	sandy mud	43.15	31.02	74.18	25.80	0	1.96
AZS13	627	sandy mud	32.40	33.18	65.58	34.40	0	3.49
AZS14	745	silty sand	18.80	30.16	48.96	51.04	0	3.08
AZS15	855	mud	43.61	48.27	91.88	8.12	0	2.98
AZS16	900	mud	41.22	49.78	90.00	9.10	0	2.75
Max.			50.27	49.86	91.88	69.36	3.14	3.49
Min.	-	-	11.22	16.27	27.49	6.76	0	1.67
Average			33.47	36.54	69.96	29.61	0.20	2.72

These facies are characterized by pale-yellow to light brown coloration, partly mottled with dark-brown and white shades, and occasionally exhibit parallel lamination (Fig. 4 (a)). The sandy mud facies contain excessive amounts of calcite grains, individual endogenic gypsum minerals, plant fragments, and shell fragments, with extremely poor sorting and a lack of marine fossils (Fig. 5 (a)). The muddy facies exhibit alternating horizontal layers of light green to dark grey-colored silty clay, with poor sorting and thickness ranging from 30 to 220 cm (Figs. 2 and 4 (b)). These facies are dominated by marine fossils (ostracod and foraminifera), as well as a high proportion of plant and root fragments (Fig. 5 (b)). The silty sand facies, with a maximum thickness of 90 cm, is less extensive compared to the muddy and sandy mud facies within the AZS and AM cores (Fig. 2). Silty sand facies are characterized by unconsolidated, lightly gray silty sand, with alternating silt and fine to medium sand, poor sorting, and an unclear and irregular boundary with the underlying facies (Fig. 4). These facies contain major minerals such as quartz, feldspar,

Table 2. Results obtained from grain size analysis of the AM core sediments.

Sample No.	Depth (cm)	Facies	Clay (%)	Silt (%)	Mud (%)	Sand (%)	Gravel (%)	Sorting
AM1	75	sandy mud	37.10	43.50	80.60	18.35	1.05	2.66
AM2	100	sandy mud	40.03	37.15	77.18	21.85	0.97	2.95
AM3	140	slightly gravelly sandy mud	44.13	32.43	76.56	20.93	2.49	3.13
AM4	200	sandy mud	32.70	35.90	68.60	31.40	0	3.10
AM5	285	sandy mud	36.81	38.10	74.91	25.08	0	2.80
AM6	300	sandy mud	28.17	42.70	70.87	28.13	1	2.84
AM7	385	mud	68.30	22.63	90.93	9.06	0	1.98
AM8	425	mud	35.23	55.47	90.70	9.29	0.92	1.87
AM9	475	mud	50.57	39.66	90.23	9.76	0	1.67
AM10	560	sandy mud	28.04	40.53	68.57	30.45	0.98	2.83
AM11	600	sandy mud	21.20	40.65	61.85	37.25	0.90	2.93
AM12	655	sandy mud	20.40	41.06	61.46	37.62	0.90	2.89
AM13	675	sandy mud	38.40	50.79	89.19	10.81	0	2.23
AM14	800	mud	40.54	48.63	89.17	10.02	0.80	2.22
Max.			68.30	55.47	90.93	37.62	2.49	3.13
Min.	-	-	20.40	22.63	61.46	9.06	0	1.67
Average			37.26	40.66	77.92	21.43	0.72	2.58

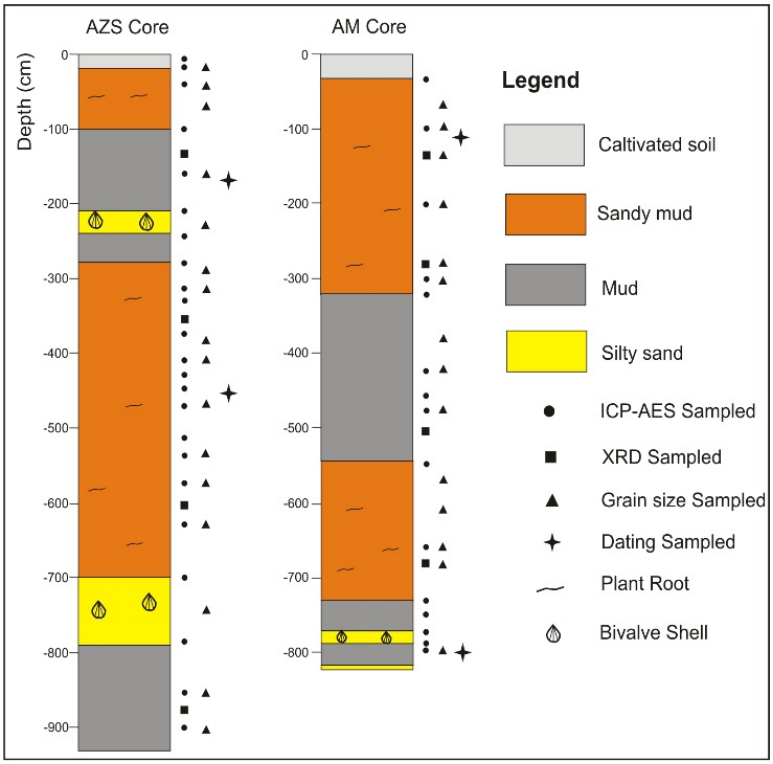

Figure 2. Lithostratigraphy columns of cores AZS and AM in the Jouybar and Zaghmarz areas (The location of two cores is shown in Fig. 1).

and rock fragments lower to moderate amounts of calcite, mica, and magnetite minerals, with well-sorted and poorly to moderately rounded clasts (Fig. 5 (c), (d)).

3. Materials and methods

Detailed field investigations were conducted on two core sediments from the Jouybar and Zaghmarz areas in the South Coast of the Caspian Sea, Mazandaran (northern Iran). The rotary drilling machine was used to obtain cores AZS and AM, with depths of 9.3 m and 8.2 m, respectively, during the 2016 and 2017 fieldworks. To characterize the grain size and sediment types, 20 core sediment samples were analyzed using wet sieving. The sediment samples were then classified according to Folk (1974)'s diagram. In order to perform dating, layers rich in organic matter were carefully sampled to prevent contamination by plant roots. Four samples, including ostracod, from different depths of the cores were analyzed for radiocarbon analysis by Accelerator Mass Spectrometry at the University of Waterloo, Canada, and the results were calibrated by the OxCal pro-

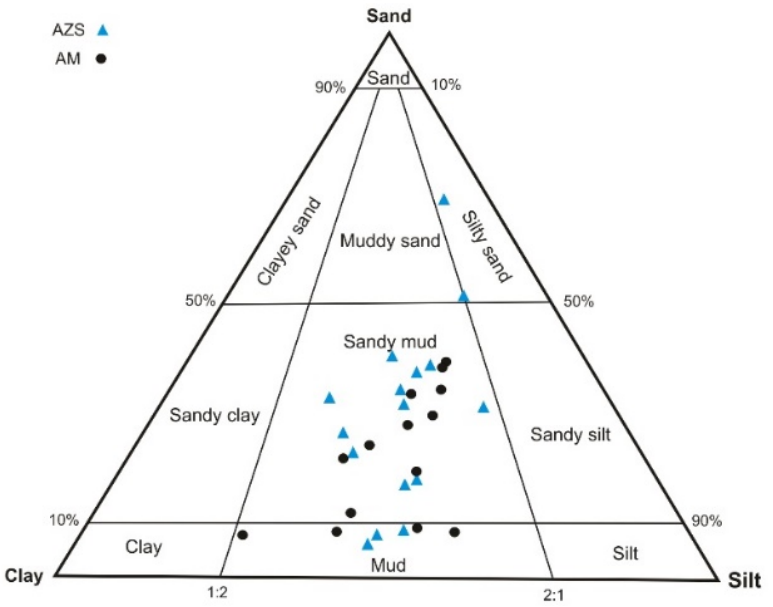

Figure 3. Classification of the AZS and AM core sediments based on Folk (1974)'s diagram.

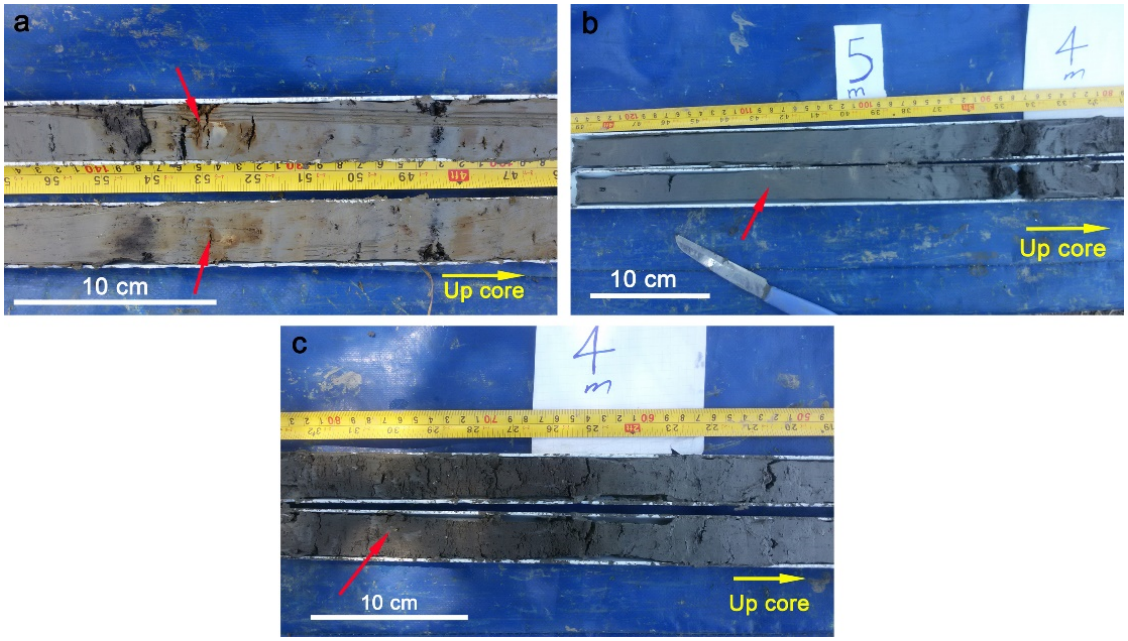

Figure 4. Field photograph of the studied facies, (a) light brown sandy mud in the core AZS, (b) light green to dark gray muddy facies in the core AM, and c) light gray silty sand in the core AZS.

gram. Additionally, forty-six representative samples were collected from two cores at different depths of the sedimentary column (Tables 3 and 4) for XRD (8 samples) and whole-rock geochemical (38 samples) analysis: 26 samples from sandy mud, 15 samples from muddy, and 5 samples from silty sand (Fig. 2, Tables 4 and 5). Post-collection, the samples were properly sealed to avoid weathering influence and external contamination. Subsequently, the samples were dried and powdered to less than 200 mesh using an agate mortar. The mineralogy of the whole-rock powder ($< 2\ \mu$m) of 8 samples was studied by X-ray diffraction (XRD) at the Geological Survey and Mineral Exploration

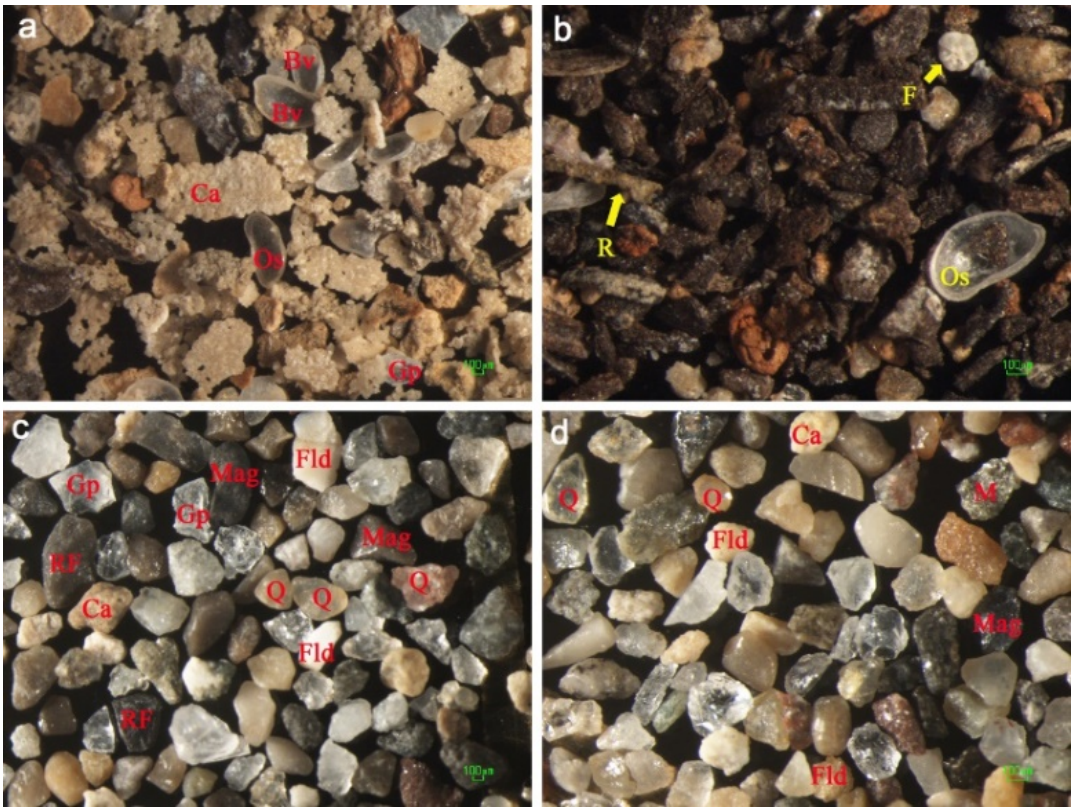

Figure 5. Images of selected samples of (a) Sandy mud, (b) Muddy, (c) and (d) Silty sand facies. Scale bar 100 μm. (Q: Quartz, Fld: Feldspar, RF: Rock Fragment, M: Mica, Ca: calcite, Gp: Gypsum, Mag: Magnetite, Bv: Bivalve, Os: Ostracod, F: Foraminifera, R: Root).

Table 3. Analytical data of major elements (in wt.%), elemental ratio, and chemical indicators of the AZS core sediments.

Sample No.	Depth (cm)	Facies	SiO_2	Al_2O_3	CaO	Fe_2O_3	MgO	K_2O	Na_2O	TiO_2	P_2O_5	MnO	LOI*	CIA	CIW	PIA	ICV	Al_2O_3/Na_2O
AZS 1	5	sandy mud	43.81	15.71	8.05	7.49	2.29	2.98	0.95	0.80	0.18	0.13	17.56	71.14	83.35	79.90	1.09	13.47
AZS 2	20	sandy mud	37.12	13.28	15.9	6.36	2.17	2.38	1.13	0.67	0.16	0.11	19.91	67.84	78.12	74.22	2.32	11.75
AZS 3	35	sandy mud	47.04	16.36	6.70	8.14	2.44	3.10	1.37	0.98	0.19	0.14	12.62	67.49	78.37	74.22	0.92	11.92
AZS 4	100	sandy mud	51.51	19.19	1.66	8.42	2.47	3.65	1.43	0.93	0.18	<0.1	9.27	68.88	80.30	76.38	<0.1	13.41
AZS 5	155	mud	47.71	17.82	4.31	10.04	2.18	3.50	1.50	0.89	0.15	<0.1	10.32	67.13	78.32	73.98	<0.1	11.89
AZS 6	210	mud	49.55	18.22	2.79	10.02	2.27	3.69	1.41	0.96	0.22	<0.1	9.45	67.78	79.63	75.31	<0.1	12.86
AZS 7	245	silty sand	45.04	14.05	10.98	5.79	2.29	2.52	2.17	0.92	0.18	0.10	14.25	58.66	66.23	61.22	1.58	6.45
AZS 8	275	mud	42.90	12.23	13.52	5.11	2.19	1.98	2.72	0.91	0.20	0.10	15.44	52.37	57.68	52.90	2.17	4.48
AZS 9	310	sandy mud	49.42	18.23	2.85	7.40	2.45	3.57	1.70	0.86	0.16	<0.1	11.45	65.80	76.49	71.93	<0.1	10.70
AZS 10	325	sandy mud	40.96	13.89	12.56	6.32	2.13	2.31	1.95	0.81	0.18	0.13	16.98	60.84	68.35	63.89	1.80	7.10
AZS 11	348	sandy mud	44.31	14.38	9.35	9.09	2.54	2.83	1.32	0.82	0.19	0.21	14.03	65.93	76.70	72.15	1.36	10.83
AZS 12	410	sandy mud	48.18	15.52	7.55	6.50	2.86	3.02	1.58	0.89	0.17	<0.1	12.44	64.60	74.80	70.07	<0.1	9.76
AZS 13	425	sandy mud	49.84	18.77	1.71	6.73	3.27	3.43	1.82	0.79	0.15	<0.1	11.16	65.87	75.74	71.46	<0.1	10.27
AZS 14	450	sandy mud	43.98	14.04	11.74	6.34	2.43	2.60	1.66	0.83	0.15	0.10	14.62	62.81	71.89	67.14	1.68	8.41
AZS 15	470	sandy mud	45.27	15.91	8.89	8.45	2.30	3.09	1.46	0.93	0.16	0.11	12.67	66.06	76.73	72.25	1.19	10.85
AZS 16	515	sandy mud	51.80	15.11	7.35	6.96	2.63	2.99	1.68	1.03	0.18	0.14	9.08	63.25	73.17	68.18	1.06	8.97
AZS 17	530	sandy mud	44.87	16.00	9.20	8.22	2.35	2.99	1.40	0.94	0.17	0.13	12.95	67.09	77.65	73.47	1.22	11.43
AZS 18	570	sandy mud	44.72	13.72	12.29	6.94	2.23	2.59	1.60	0.84	0.16	0.11	14.08	62.89	72.16	67.35	1.79	8.53
AZS 19	627	sandy mud	42.89	12.07	14.69	6.98	2.45	2.55	1.50	0.84	0.18	0.17	14.93	61.02	70.91	65.28	2.38	8.02
AZS 20	700	sandy mud	43.49	12.78	13.31	7.45	2.39	2.59	1.45	0.80	0.19	0.13	14.65	62.76	72.78	67.61	2.06	8.80
AZS 21	780	silty sand	51.82	14.71	5.53	7.30	2.56	2.94	1.88	0.84	0.20	<0.1	10.99	61.04	70.34	65.01	<0.1	7.80
AZS 22	855	mud	40.45	11.49	17.49	5.82	2.29	2.08	1.48	0.74	0.16	0.10	17.13	61.62	70.12	65.33	2.91	7.72
AZS 23	900	mud	43.50	12.81	14.72	6.80	2.32	2.52	1.5	0.78	0.16	0.11	14.08	62.55	72.20	67.13	2.25	8.54
Min.	-	-	37.12	11.49	1.66	5.11	2.13	1.98	0.95	0.67	0.15	0.10	9.08	52.37	57.68	52.90	0.92	4.48
Max.	-	-	51.82	19.19	17.49	10.04	3.27	3.69	2.72	1.03	0.22	0.17	17.56	71.14	83.35	79.90	2.91	13.47

Litho: Lithology; *LOI: loss on ignition; CIA = $[Al_2O_3/(Al_2O_3+CaO^*+Na_2O+K_2O)] \times 100$ (Nesbitt and Young, 1982); CIW = $[Al_2O_3/(Al_2O_3+CaO^*+Na_2O)] \times 100$ (Harnois, 1988); PIA = $[(Al_2O_3-K_2O)/(Al_2O_3+CaO^*+Na_2O-K_2O)] \times 100$ (Fedo et al., 1995). ICV = $[Fe_2O_3+K_2O+Na_2O+CaO+MgO+MnO+TiO_2]/Al2O_3$ (Cox et al., 1995).

in Tehran, Iran. Thirty-eight representative samples from cores AZS and AM have been selected for their major and trace-element analyses. The concentrations of major and some trace elements were measured using Inductively Coupled Plasma-Atomic Emission Spectroscopy (ICP-AES) at the Geological Survey and Mineral Exploration of Iran. The samples were accurately quantified (50 mg) and put into the muffle furnace at 500 °C for 2 hours. The samples were then digested in a mixed solution of $HCl+HClO_4+HF+HNO_3$ for two hours, filtered into bottles, and left to stand for 24 hours. The chemical index of alteration (CIA; (Nesbitt and Young, 1982)), the chemical index of weathering (CIW; (Harnois, 1988)), the plagioclase index of alteration (PIA; (Fedo et al., 1995)), and the index of compositional variability (ICV; (Cox et al., 1995)) were used to determine the intensity of chemical weathering and compositional maturity, respectively.

Dating

Four samples of Ostracod fossils were collected from mud and sandstone facies. These samples included two from the AZS core, at depths of 175 cm and 460 cm, respectively, and two from the AM core, at depths of 115 cm and 850 cm, respectively. The age of these samples was determined using the carbon-14 method. The carbon-14 ages of the AZS and AM core samples are 1917, 2320, 1498, and 4455 years, respectively (Table 5). Table 5 and figure 2 demonstrate that all four carbon-14 ages are consistent with the stratigraphic

Table 4. Analytical data of major elements (in wt.%), elemental ratios, and chemical indicators of the AM core sediments.

Core	Depth (cm)	Facies	SiO_2	Al_2O_3	CaO	Fe_2O_3	MgO	K_2O	Na_2O	TiO_2	P_2O_5	MnO	LOI*	CIA	CIW	PIA	ICV	Al_2O_3/Na_2O
AM1	30	sandy mud	38.96	12.77	15.19	6.07	2.60	2.49	1.59	0.77	0.12	<0.1	19.49	61.73	70.97	65.86	0.50	8.04
AM2	100	sandy mud	41.07	9.88	19.66	4.88	2.26	1.79	1.59	0.78	0.16	<0.1	18.35	57.93	65.34	60.26	0.58	6.20
AM3	200	sandy mud	38.49	10.43	19.91	4.08	2.05	1.88	1.64	0.70	0.11	<0.1	21.18	58.37	65.89	60.84	0.57	6.36
AM4	300	sandy mud	40.09	12.27	16.37	6.61	2.31	2.44	1.60	0.98	0.13	<0.1	17.48	60.76	69.92	64.58	0.54	7.65
AM5	325	sandy mud	38.82	12.48	17.30	6.27	2.28	2.46	1.45	0.83	0.13	<0.1	18.37	62.71	72.37	67.34	0.54	8.62
AM6	425	mud	32.49	9.99	22.84	5.51	2.33	1.90	1.73	0.61	0.10	<0.1	20.74	56.32	63.73	58.24	0.63	5.78
AM7	455	mud	26.48	6.22	31.13	3.16	1.77	1.20	1.51	0.45	<0.1	<0.1	27.25	49.79	55.57	49.73	0.75	4.12
AM8	475	mud	37.04	11.54	19.58	5.64	2.31	2.21	1.62	0.83	0.11	0.10	18.58	59.96	68.46	63.25	0.58	7.14
AM9	545	mud	30.50	5.66	30.05	2.42	1.96	1.01	1.79	0.53	<0.1	<0.1	25.01	44.75	48.97	43.66	0.76	4.16
AM10	655	Sandy mud	35.31	10.59	21.51	4.82	2.76	2.03	1.40	0.73	0.10	0.13	20.49	60.95	69.77	64.66	0.62	7.59
AM11	730	Sandy mud	37.68	11.76	18.25	6.59	2.83	2.27	1.25	0.78	<0.1	0.14	19.25	64.13	74.08	69.32	0.57	9.40
AM12	750	mud	31.40	8.17	26.10	4.13	2.19	1.45	1.64	0.52	0.10	<0.1	23.66	53.94	60.18	54.97	0.67	4.97
AM13	775	mud	35.08	10.00	22.31	4.68	2.34	1.89	1.47	0.77	0.10	0.10	20.81	59.19	67.33	62.12	0.63	6.78
AM14	787	silty sand	43.79	12.55	14.78	6.61	2.41	2.24	1.61	0.89	0.14	0.12	15.44	61.94	70.35	65.69	0.51	7.80
AM15	800	mud	44.45	9.67	18.36	3.89	2.16	1.96	2.20	0.63	0.15	<0.1	16.54	50.82	57.21	51.05	0.55	4.40
Min.	-	-	26.48	6.22	14.78	2.42	1.77	1.01	1.25	0.45	0.10	0.1	15.44	44.75	48.97	43.66	0.50	4.12
Max.	-	-	44.45	12.77	31.13	6.61	2.83	2.49	2.20	0.98	0.16	0.14	27.25	64.13	74.08	69.32	0.76	9.40

Table 5. Carbon 14 dating results and recalibrated ages related to the studied samples from two selected cores.

Core	Facies	Sample depth (cm)	Carbon 14	Sample age (years)	Calibrated age with σ1 range
AZS	Mud	175	78.77	1917	27
AZS	Sandy Mud	460	74.92	2320	27
AM	Sandy Mud	115	82.99	1498	35
AM	Mud	800	57.43	4455	50

order, indicating a continuous sedimentary history dating back to approximately 4455 years ago. Age determination with carbon-14 isotope in AM and AZS cores were also applied to determine the sedimentation rate. The average sedimentation rate in AM and AZS cores is around 1.6 mm per year.

4. Result and discussion

4.1 Bulk mineralogy

Clay minerals are widely used to find the origin of and reconstruct weathering conditions in marine and lake environments (Campo et al., 2007). The origin of clay minerals involves both primary (debris) during physical erosion and chemical weathering of source rocks, as well as secondary minerals (degradation) formed from diagenetic changes after deposition. Consequently, the distribution of clay minerals in modern sediments reflects the climate and intensity of weathering in the source area (Chamley, 1989).

X-ray diffraction (XRD) analysis was utilized to determine the bulk mineralogy of eight powdered samples from sandy mud and muddy units (Fig. 2). Figure 6 illustrates the X-ray diffraction patterns of the brown sandy mud facies of the AZS core (depth 350 cm) and the dark mud facies of the AM core (depth 500 cm) from Jouybar and Zaghmarz areas, respectively, in the southern coasts of the Caspian Sea. In figure 6, the strong peaks of 3.67, 3.02, 2.27, and 2.88 Å confirm the abundant presence of calcite and dolomite in these samples. The peaks of 24.4 and 3.33 Å indicate the presence of quartz. Feldspar and secondary minerals (hematite) are characterized by peaks of 4.13 and 3.19 Å, and 2.56 and 91.9 Å, respectively (Fig. 6 (a), (b)). Weak peaks of 14.02 and 4.69 Å suggest the presence of smectite and chlorite. The peak at 56.7 Å represents the first-order peak of kaolinite and the second-order peak of chlorite. Comparing the relative intensity of the most prominent peak of each component, quartz, illite, mica, feldspar, and calcite appear to be the most abundant minerals (Fig. 6 (a), (b)). The clay fraction includes illite, kaolinite, smectite, and chlorite minerals (Fig. 6 (a), (b)).

Therefore, the dominant presence of sedimentary rocks (shale, sandstone, marl, and massive limestone), volcanic rocks (basaltic and andesite), and metamorphic rocks in the southern parts of the Jouybar and Zaghmarz areas can strongly explain the presence of clastic, carbonate minerals (calcite and dolomite), and clay minerals (such as chlorite and smectite) in the studied samples. The amount of calcium carbonate (calcite) indicates the paleoclimatic conditions (Yunfei, 1993; Das et al., 2006). The excessive amount of calcium carbonate in the samples indicates the prevailing arid weather conditions in the region. Additionally, the presence of primary and secondary calcite and gypsum minerals, along with unstable components such as feldspar and pebbles in the sandstone and silty sand facies (Fig. 5 (a), (c), (d)), is confirmed to be a result of arid and semi-arid weather conditions during the deposition of these facies. Furthermore, the presence of calcite, dolomite, as well as illite, chlorite, and smectite clay minerals in the

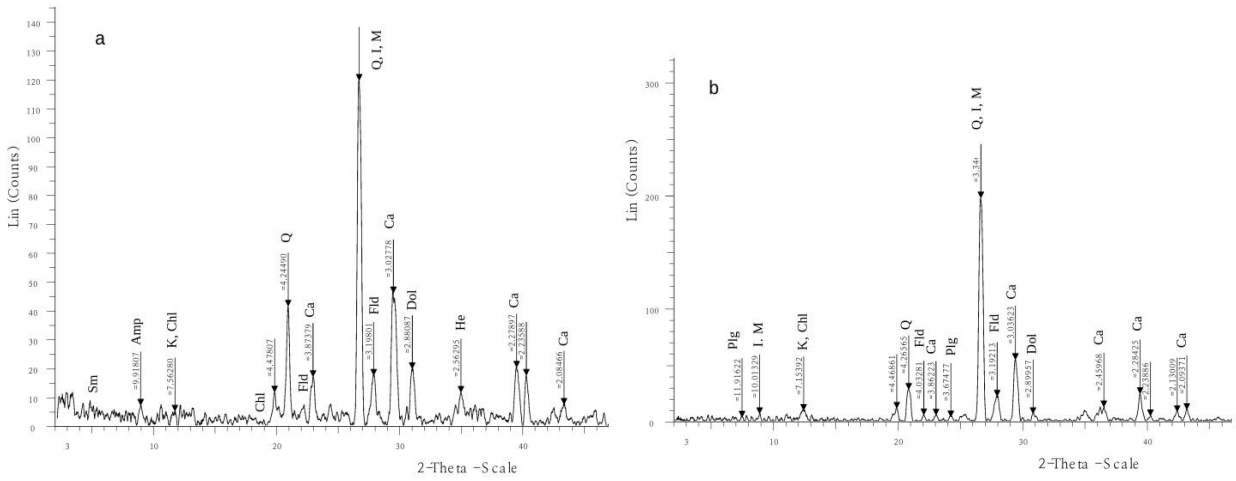

Figure 6. X-ray diffraction patterns of representative bulk samples from (a) brown sandy mud facies (3.5 m depth) in AZS core, and (b) dark muddy facies (5 m depth) in AM core (Q: Quartz, I: Illite, M: Mica, Fld: Feldspar, Ca: Calcite, Dol: Dolomite, K: Kaolinite, Chl: Chlorite, Sm: Smectite, Plg: Plagioclase, He: Hematite).

studied samples, indicates arid and semi-arid climatic conditions (Dixon and Weed, 1992). Smectite clay minerals are also indicators of arid climatic conditions with wet seasons (Chamley, 1989), which corresponds to the semi-arid climatic conditions during the deposition of the studied facies. The mineralogical composition results obtained from the XRD patterns indicate that the selected samples are similar, indicating a common source for the core sediments.

4.2 Major element

Environmental conditions have an impact on the chemical properties of elements and compounds. Changes in sediment geochemistry can indicate fluctuations in paleoenvironmental conditions during sedimentation and diagenesis. Consequently, the major elements found in sediments, namely SiO_2, K_2O, CaO, MgO, Na_2O, Al_2O_3, Fe_2O_3, and TiO_2, serve as useful indicators for determining paleoenvironmental conditions (Wei et al., 2015). The concentrations of major elements in sandy mud, muddy, and silty sand facies at various depths from the AZS and AM cores are provided in Tables 4 and 5, respectively. SiO_2 is the most abundant oxide in all samples, with an average content of 45.58% and 38.63% in sandy mud, 45.92% and 33.92% in muddy, and 45.77% and 43.79% in silty sand facies from the AZS and AM cores, respectively. The second most abundant oxide is Al_2O_3, with average contents of 15.31% and 11.45% in sandy mud, 15.27% and 8.75% in muddy, and 13.42% and 12.55% in silty sand facies from the AZS and AM cores, respectively. Following Al_2O_3, the next most abundant oxide is CaO, with average contents of 8.99% and 18.31% in sandy mud, 8.84% and 24.34% in muddy, and 11.33% and 14.78% in silty sand facies from the AZS and AM cores, respectively. Fe_2O_3 is the next most abundant oxide, with average contents of 7.36% and 5.62% in sandy mud, 7.99% and 4.20% in muddy, and 6.30% and 6.61% in silty sand facies from the AZS and AM cores, respectively. The average contents of MgO are 2.46% and 2.44% in sandy mud, 2.92% and 2.15% in muddy, and 2.36% and 2.41% in silty sand facies from the AZS and AM cores, respectively. The average contents of K_2O are 2.92% and 2.19% in sandy mud, 2.92% and 1.66% in muddy, and 2.51% and 2.24% in silty sand facies from the AZS and AM cores, respectively, while the average contents of Na_2O are 1.50% and 1.50% in sandy mud, 1.78% and 1.71% in muddy, and 1.84% and 1.61% in silty sand facies from the AZS and AM cores, respectively. These findings are broadly consistent with the indications from XRD analysis (Fig. 6). On the other hand, the contents of other oxides, including TiO_2, P_2O_5, and MnO, are less than 1.0%. Therefore, the abundance of oxide compounds in the studied cores follows the sequence: $SiO_2 > Al_2O_3 > CaO > Fe_2O_3 > MgO > K_2O > Na_2O > TiO_2 > P_2O_5 > MnO$. Al_2O_3 is considered immobile during weathering and sedimentation; therefore, the abundance of major and some trace elements is plotted against Al_2O_3 to investigate the primitive geochemical nature (McLennan et al., 1993; Cardenas et al., 1996; Bauluz et al., 2000). The positive correlations between K_2O, Fe_2O_3, SiO_2, and TiO_2 with Al_2O_3 (with correlation coefficients R of 0.93, 0.65, 0.53, and 0.47, respectively) in the sediments of the AZS and AM cores (Fig. 7 (a-d)) suggest that these elements are predominantly hosted in clay minerals, particularly illite, or are derived from detrital sediments (McLennan et al., 1983; Das et al., 2006; Lee, 2009). The negative correlation between CaO and Al_2O_3 (with a correlation coefficient R of -0.90) (Fig. 7 (e)) indicates that CaO is not associated with Al-bearing minerals and may originate from carbonate rock fragments (Rahman and Suzuki, 2007; Lee, 2009). The sediments of both cores have a high concentration of CaO, indicating the predominance of arid paleoclimate conditions with evaporation in the basin (Gromet et al., 1984; Sun et al., 2012). There is no obvious correlation between other major oxides, such as Na_2O and Al_2O_3 (Fig. 7 (f)).

4.3 Trace elements

The distribution of elements in sediments or sedimentary rocks is influenced by paleoclimate and environmental processes, making their trace element ratios particularly useful for studying paleoclimate (**Bailey1996**; Song et al., 2016). The concentrations and ratios of trace elements in the sandy mud, muddy, and silty sand facies at different depths from the AZS and AM cores are listed in Tables 6 and 7, respectively. The data for trace elements show high values of Sr (average 774.57 and 169.14 ppm in sandy mud, 682.88 and 160.76 ppm in muddy, and 688.74 and 173.00 ppm in silty sand facies from the AZS and AM cores, respectively), Zr (average 248.25 and 73.71 ppm in sandy mud, 249.73 and 76.00 ppm in muddy, and 220.39 and 63.00 ppm in silty sand facies from the AZS and AM cores, respectively), Cr (average 243.57 and 100.29 ppm in sandy mud, 257.12 and 84.00 ppm in muddy, and 227.61 and 83.00 ppm in silty sand facies from the AZS and AM cores, respectively), Rb (average 212.40 and 79.71 ppm in sandy mud, 188.47 and 86.14 ppm in muddy, and 188.60 and 70.00 ppm in silty sand facies from the AZS and AM cores, respectively), and V (average 137.53 and 103.71 ppm in sandy mud, 134.91 and 104.43 ppm in muddy, and 118.48 and 93.00 ppm in silty sand facies from the AZS and AM cores, respectively) (Tables 6 and 7).

The bivariate relationship between some trace elements (Sc, V, Hf, Th, and Rb) and Al_2O_3 is shown in Fig. 8. Strong to moderate positive correlations between Sc, V, and Hf with Al_2O_3 ($R = 0.92$, 0.91, and 0.51, respectively) in the sediments of AZS and AM cores (Fig. 8 (a-c)) indicate their association with clay minerals (Roy and Roser, 2012) (Fig. 6). The low or negative relationship of Al_2O_3 with Th and Rb (Fig. 8 (d), e), suggests that their fractions are not related to clay mineral contents (Roy and Roser, 2012).

Various discrimination diagrams based on major oxide concentrations in clastic sediments exist (Pettijohn et al., 2012; Herron, 1988). Among these, log (Na_2O/K_2O) and log (Fe_2O_3/K_2O) vs. log (SiO_2/Al_2O_3) classification diagrams proposed by Pettijohn et al. (2012) and Herron (1988) have been used. Based on these plots, the samples from the AZS and AM cores can be classified as greywacke, litharenite, and shale lithologies (Fig. 9).

4.4 Paleoweathering and paleoclimate

Generally, the high values of the chemical alteration of the source area are attributed to the omission and leaching of

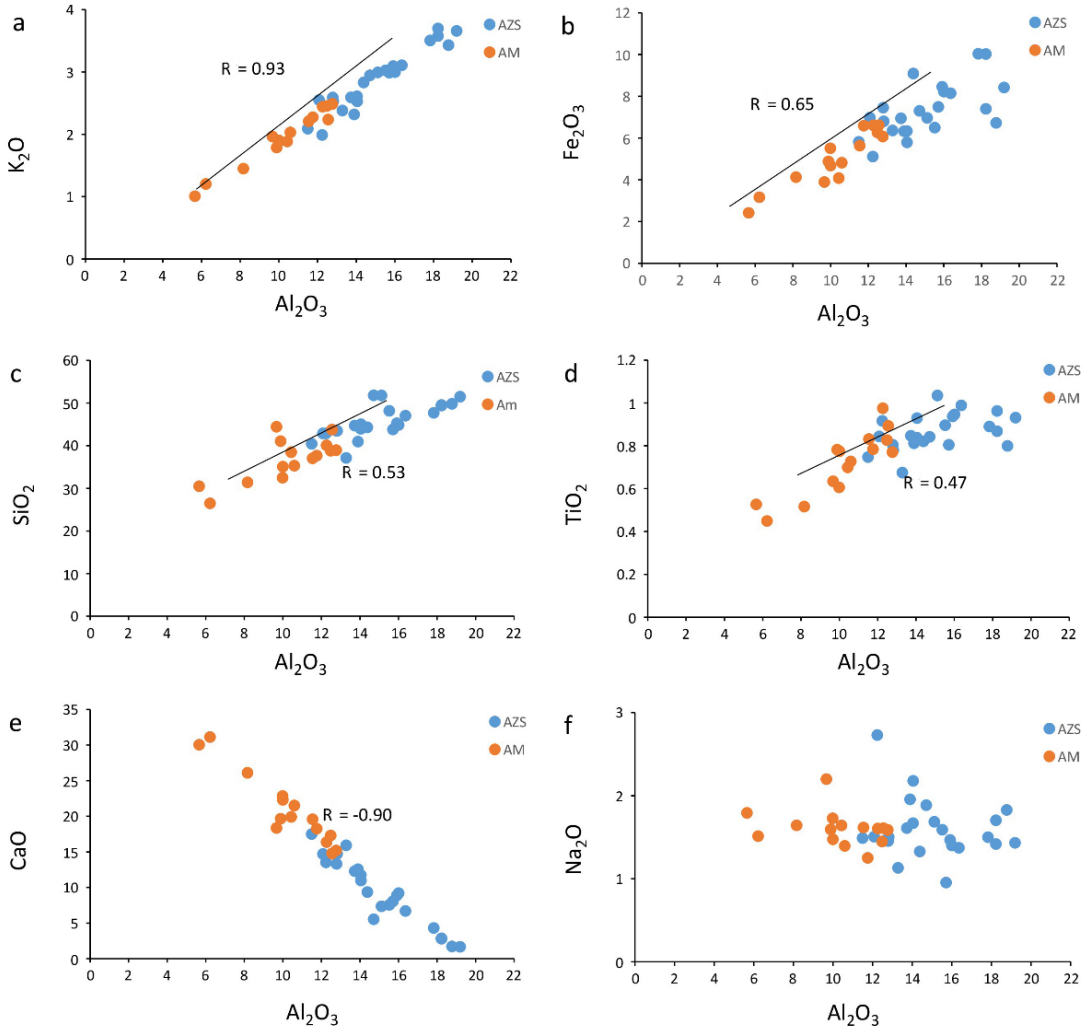

Figure 7. The diagram of variation of major elements plotted against Al2O3 for the investigated sediments from the AZS and AM cores.

mobile cations (e.g., Ca^{+}, Na^{+}, and K^{+}) from the sediments in relation to the less mobile or residual constituents (Al^{3+}, Ti^{4+}, and Si^{4+}) (Nesbitt and Young, 1982; Fedo et al., 1996; Cingolani et al., 2003). Therefore, the intensity of chemical weathering of source rocks and sedimentary recycling can be determined by analyzing the composition of sediments (Nesbitt and Young, 1982; Armstrong-Altrin et al., 2004; Lee, 2009).

Three weathering indexes, namely the Chemical Index of Alteration (CIA), Chemical Index of Weathering (CIW), and Plagioclase Index of Alteration (PIA), as presented by Nesbitt and Young (1982), Harnois (1988), and Fedo et al. (1995) respectively, are applied to study the degree and intensity of chemical alteration of the AZS and AM core sediments.

In the CIA formula, CaO* represents the Ca content in silicate-bearing minerals (Nesbitt and Young, 1982) and is calculated as $CaO^* = CaO - 10/3 \times P_2O_5$, as reported by McLennan et al. (1993). In this study, CaO was corrected according to the method proposed by McLennan et al. (1993), where CaO values are accepted only if $CaO < Na_2O$. If $CaO > Na_2O$, it is assumed that the concentration of CaO is equal to Na_2O.

Generally, low, moderate, and high CIA values (< 60, $60 - 80$, and > 80) depict cold and dry, warm and humid, and hot and humid climate conditions, respectively, in which the sediments undergo weak, medium, and intensive chemical weathering (Nesbitt and Young, 1982; Fedo et al., 1995; Yan et al., 2010; Fu et al., 2015; Ma et al., 2015). CIA values of the sandy mud, muddy, and silty sand sediments from the AZS and AM cores are given in Tables 4 and 5, respectively. In the studied samples, the CIA values range from 60.84 to 71.14 (avg. 65.27) and 57.93 to 64.13 (avg. 60.94) in sandy mud, 52.37 to 67.78 (avg. 62.46) and 44.75 to 59.96 (avg. 53.54) in muddy, and 58.66 to 61.04 (avg. 60.44) and 61.94 in silty sand facies from AZS and AM cores, respectively (Tables 4 and 5), indicating weak to moderate chemical weathering in the source areas.

The CIW values proposed by Harnois (1988) are used to assess the intensity of chemical weathering in the source area. In the CIW formula, the CaO* contents were also calculated according to McLennan et al. (1993). The CIW values of the studied sediments range from 68.35 to 83.35 (avg. 75.47) and 65.34 to 74.08 (avg. 69.76) in sandy mud, 57.68 to 79.63 (avg. 71.96) and 48.97 to 68.46 (avg. 60.21) in muddy, and 66.23 to 70.12 (avg. 68.90) and 70.35 in silty

2008-8779[https://doi.org/10.57647/j.ijes.2025.16794]

Table 6. Some selected trace element concentrations (in ppm) and their ratios of the AZS core sediments.

Core	Litho.	Co	Cu	Cr	Hf	La	Ni	Sc	Sr	Th	V	Zr	Rb	U/Th	V/Cr	Ni/Co	Sr/Cu	Rb/Sr	Zr/Sc	Th/Sc
AZS 1	sandy mud	17.41	39.47	243.28	9.15	91.35	107.61	76.20	1000.78	24.76	140.51	246.29	274.23	0.42	0.58	6.18	25.36	0.27	3.23	0.32
AZS 2	”	13.78	37.05	206.85	9.68	79.05	87.54	64.27	1762.43	24.41	115.32	242.68	485.66	0.42	0.56	6.35	47.56	0.28	3.78	0.38
AZS 3	”	19.47	38.83	256.41	17.07	99.36	113.55	78.63	1148.06	24.08	144.50	262.51	320.01	0.39	0.56	5.83	29.57	0.28	3.34	0.31
AZS 4	”	22.62	50.24	311.60	25.71	104.23	139.00	90.81	591.78	21.60	179.28	269.01	165.74	0.47	0.58	6.14	11.78	0.28	2.96	0.24
AZS 5	mud	18.55	36.20	291.56	34.44	93.01	122.05	81.58	583.86	24.10	164.04	264.93	163.30	0.46	0.56	6.58	16.13	0.28	3.25	0.30
AZS 6	”	20.95	44.83	290.10	21.66	101.19	122.72	89.65	540.31	23.73	169.78	255.43	147.83	0.48	0.59	5.86	12.05	0.27	2.85	0.26
AZS 7	silty sand	16.34	38.95	238.59	14.30	90.57	96.38	63.66	823.85	23.34	117.05	282.51	224.98	0.29	0.49	5.90	21.15	0.27	4.44	0.37
AZS 8	mud	14.19	33.99	229.65	14.13	76.18	78.07	47.96	981.37	21.92	91.19	245.97	274.21	0.30	0.40	5.50	28.87	0.28	5.13	0.46
AZS 9	sandy mud	19.98	44.98	292.22	23.30	102.69	125.89	86.27	655.04	22.41	165.86	247.77	181.53	0.37	0.57	6.30	14.56	0.28	2.87	0.26
AZS 10	”	15.62	34.74	209.35	15.13	81.12	85.39	59.95	1179.18	23.31	110.46	218.87	320.62	0.34	0.53	5.47	33.95	0.27	3.65	0.39
AZS 11	”	17.78	35.40	229.72	15.35	84.27	103.28	69.28	546.07	26.32	137.42	271.95	148.65	0.48	0.60	5.81	15.42	0.27	3.93	0.38
AZS 12	”	18.79	35.44	246.92	15.16	90.82	115.71	76.34	543.31	23.48	147.43	265.34	147.26	0.36	0.60	6.16	15.33	0.27	3.48	0.31
AZS 13	”	21.52	52.55	306.49	22.30	106.21	125.76	89.09	550.01	21.21	172.88	283.81	151.77	0.41	0.56	5.84	10.47	0.28	3.19	0.24
AZS 14	”	15.98	35.19	223.46	17.37	87.09	95.85	64.73	945.65	23.40	123.10	239.37	254.95	0.34	0.55	6.00	26.87	0.27	3.70	0.36
AZS 15	”	21.78	40.20	258.21	14.87	97.24	115.01	78.70	512.26	25.62	145.22	258.02	143.17	0.39	0.56	5.28	12.74	0.28	3.28	0.33
AZS 16	”	22.59	34.71	237.74	13.89	84.97	113.51	68.05	723.37	22.41	126.26	191.66	198.49	0.40	0.53	5.02	20.84	0.27	2.82	0.33
AZS 17	”	19.78	50.75	259.66	15.05	97.58	116.96	80.26	573.32	25.65	145.41	250.46	155.76	0.39	0.56	5.91	11.30	0.27	3.12	0.32
AZS 18	”	19.22	28.76	215.22	13.94	84.31	97.07	63.18	568.27	24.28	116.91	250.90	153.37	0.38	0.54	5.05	19.76	0.27	3.97	0.38
AZS 19	”	17.42	40.40	196.88	9.23	76.37	93.13	57.75	546.28	25.09	112.55	241.89	148.60	0.34	0.57	5.35	13.52	0.27	4.19	0.43
AZS 20	”	17.14	33.13	203.11	10.81	77.67	90.99	61.59	547.24	24.49	117.36	231.44	148.65	0.38	0.58	5.31	16.52	0.27	3.76	0.40
AZS 21	silty sand	17.44	43.43	254.80	15.75	82.88	107.46	70.36	567.81	22.76	136.45	196.95	156.84	0.38	0.54	6.16	13.07	0.28	2.80	0.32
AZS 22	mud	13.61	29.77	189.43	11.50	143.13	90.24	53.37	674.55	23.66	101.94	181.71	183.98	0.30	0.54	6.63	22.66	0.27	3.40	0.44
AZS 23	”	15.14	32.48	217.17	11.38	73.50	95.37	61.27	625.97	24.44	114.62	232.58	168.55	0.32	0.53	6.30	19.27	0.27	3.80	0.40

2008-8779[https://doi.org/10.57647/j.ijes.2025.16794]

Table 7. Some selected trace element concentrations (in ppm) and their ratios of the AM core sediments.

Core	Litho.	Co	Cu	Cr	Hf	La	Ni	Sc	Sr	Th	V	Zr	Rb	U/Th	V/Cr	Ni/Co	Sr/Cu	Rb/Sr	Zr/Sc	Th/Sc
AM1	sandy mud	14.50	33.99	90	2.36	22	46	13.50	150	6.79	106	84	86	0.29	0.57	4.67	30.27	0.24	8.29	0.60
AM2	”	15.50	23.82	112	2.50	23	60	14.80	151	7.4	110	89	90	0.29	0.55	4.11	65.71	0.24	10.05	0.72
AM3	”	14.60	24.93	127	1.96	23	76	12.40	166	6.61	91	66	63	0.24	0.51	3.94	30.66	0.24	8.77	0.65
AM4	”	11.80	36.30	91	1.91	23	40	11.30	181	6.68	97	64	70	0.32	0.53	4.93	19.28	0.24	8.32	0.55
AM5	”	14.20	35.37	119	1.79	22	43	12.80	186	6.65	105	69	78	0.28	0.53	4.88	21.64	0.25	8.21	0.51
AM6	mud	14.20	30.11	87	2.24	22	45	13.00	205	6.57	101	74	79	0.29	0.48	5.25	55.58	0.25	8.89	0.68
AM7	”	16.50	16.60	92	2.06	24	49	14.60	139	7.78	117	68	95	0.21	0.35	3.77	152.47	0.25	10.00	0.99
AM8	”	14.20	88.44	81	2.02	24	43	13.00	84.3	6.60	94	70	80	0.30	0.50	4.94	11.99	0.25	8.87	0.60
AM9	”	12.80	11.91	76	2.63	23	45	14.90	175	7.81	111	93	85	0.16	0.29	3.85	197.35	0.25	11.33	1.03
AM10	Sandy mud	12.50	24.98	78	2.21	21	45	13.70	164	6.99	107	73	85	0.28	0.53	4.57	53.02	0.26	8.18	0.62
AM11	”	16.30	28.19	85	2.07	23	52	13.90	186	6.44	110	71	86	0.31	0.56	5.07	40.97	0.26	6.82	0.56
AM12	mud	9.60	19.38	80	2.28	21	36	13.30	177	7.17	105	79	92	0.29	0.40	4.75	106.23	0.26	9.85	0.75
AM13	”	14.50	24.12	86	2.41	24	51	13.60	160	7.12	103	83	87	0.29	0.56	4.64	51.54	0.26	7.90	0.61
AM14	silty sand	10.40	37.71	83	1.62	23	38	11.80	173	6.34	93	63	70	0.34	0.44	5.14	18.32	0.27	7.30	0.52
AM15	mud	12.10	16.31	86	2.04	23	42	13.20	185	6.59	100	65	85	0.28	0.38	4.82	52.45	0.28	10.14	0.62

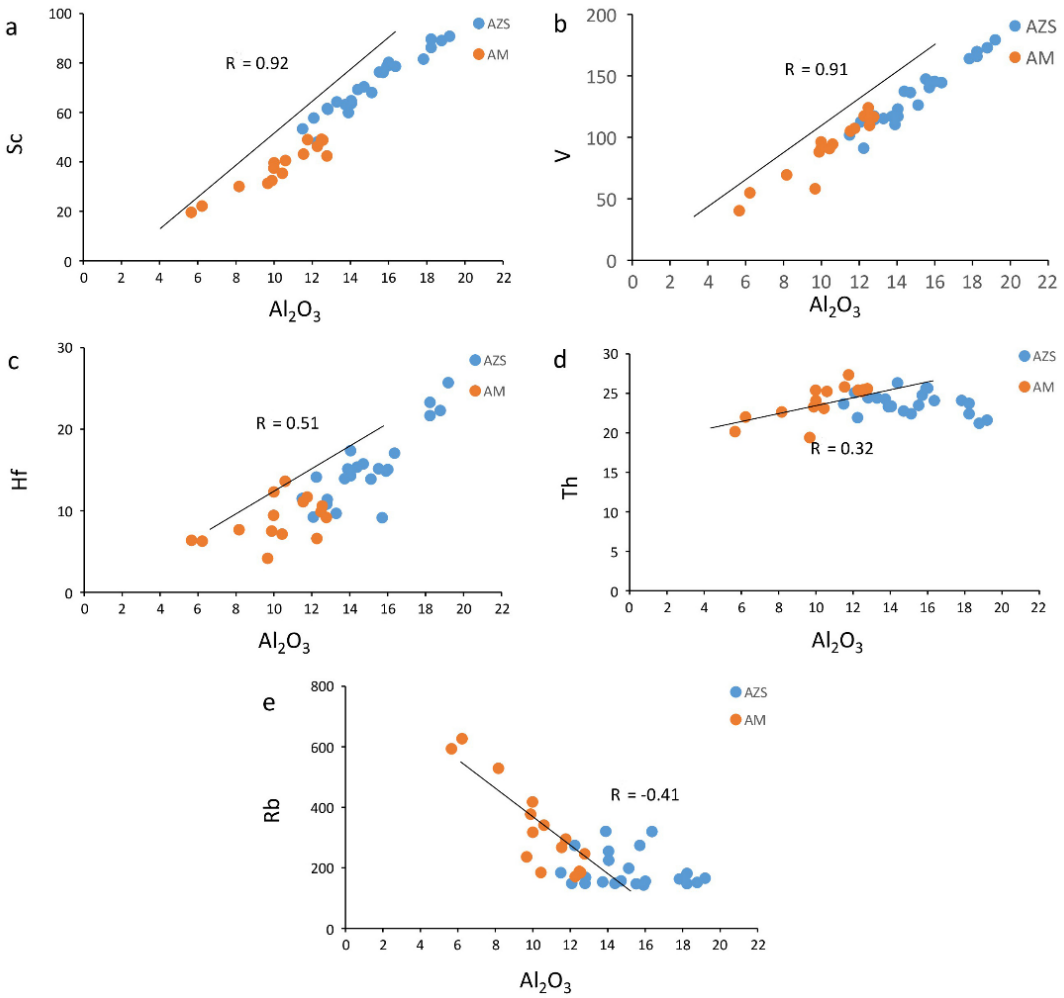

Figure 8. The diagram of variation of some trace elements plotted against Al_2O_3 for the investigated sediments from the AZS and AM cores.

sand facies from AZS and AM cores, respectively (Tables 4 and 5). This indicates weak to moderate chemical weathering with semi-arid to semi-humid climate conditions.

The degree and intensity of chemical alteration can also be inferred by calculating PIA values. PIA values range from 50 to 100 for fresh or unweathered plagioclase and secondary aluminous clay minerals (e.g., kaolinite, illite, and gibbsite), respectively (Fedo et al., 1995). Therefore, the PIA values vary from 63.89 to 79.90 (avg. 70.97) and 60.26 to 69.32 (avg. 64.69) in sandy mud, 52.90 to 75.31 (avg. 67.33) and 43.66 to 63.25 (avg. 54.72) in muddy, and 61.22 to 65.01 (avg. 63.85) and 65.69 in silty sand facies from AZS and AM cores, respectively (Tables 4 and 5). This indicates weak to moderate chemical weathering in the source region.

Likewise, according to the binary plots of Shaltami (2012), the CIW and PIA versus CIA projected values of both cores' sediments are in the low to intermediate weathering fields (Fig. 10).

The degree of chemical weathering and mobility of elements is also determined by using an Al_2O_3 (A), CaO^*+Na_2O (CN), and K_2O (K) ternary diagram in molar proportions. The CIA values can be plotted on the A-CN-K triangular diagram to interpret compositional variations related to chemical weathering, paleoclimate, and source material composition (Nesbitt and Young, 1984; Fedo et al., 1995; Fedo et al., 1996; Fedo et al., 1997a; Fedo et al., 1997b; Ghosh et al., 2012; Deepthi et al., 2013), as shown in Fig. 11 (a). The total samples from the AZS and AM cores are plotted above the K-feldspar-plagioclase join line, following a linear trend close to the A-CN join line. They display a tendency towards the A apex, indicating that these samples were not subjected to intensive chemical weathering in the source areas. A bivariate major oxides plot was also used to interpret the core samples' paleoclimate and chemical maturity, plotting SiO_2 against $Al_2O_3+K_2O+Na_2O$ (Suttner and Dutta, 1986). This plot shows that the two core samples exhibit semi-arid to semi-humid paleoclimate conditions with low chemical maturity (Fig. 11 (b)).

The results obtained from the study of chemical weathering indices (CIA, CIW, PIA) and the compositional variability index (ICV) show a low to moderate degree of weathering in the source area. Additionally, it indicates the prevalence of arid to semi-arid conditions during the deposition, which suggests an active tectonic setting in the source area (rapid uplift) and a lower sedimentary cycle for the sediments. Alborz mountain range (a branch of the Alpine-Himalayan orogenic belt) has been extensively studied using various

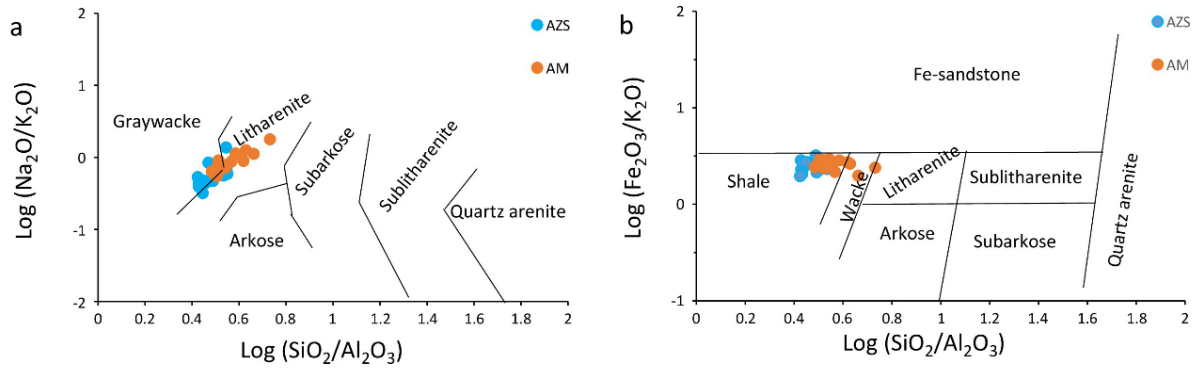

Figure 9. The diagrams of geochemical classification of AZS and AM core samples from Jouybar and Zaghmarz areas using: a) Log (Na_2O/K_2O) vs. Log (SiO_2/Al_2O_3) (Pettijohn et al., 2012) and b) Log (SiO_2/Al_2O_3) vs. Log (Fe_2O_3/K_2O) (after (Herron, 1988)).

approaches, including seismicity analysis, GPS (Global Positioning System) data, and morphotectonic indices, to document its high tectonic activity (**Tourani2024**). Based on this, it can be concluded that both the AZS and AM core sediments experienced alternating arid and semi-arid paleoclimate conditions during the Holocene period, approximately 4455 years ago.

4.4.1 Elemental ratios

Several chemical ratios, such as Sr/Cu, Rb/Sr, and Al_2O_3/Na_2O, may be considered important indicators of climate changes and source-rock weathering, which determine the characteristics of the sediment (Jin and Zhang, 2002; Chen et al., 2001; Meng et al., 2012; Bai et al., 2015; Fu et al., 2016). Therefore, low Sr/Cu and high Rb/Sr ratios in sediments are commonly associated with warm and humid climate conditions, as intense chemical weathering in warm and humid climates mostly removes Sr compared to Rb and Cu (Lerman et al., 1995; Meng et al., 2012; Cao et al., 2015). Sr/Cu ratios ranging from 1 to 10 indicate warm and humid paleoclimate conditions, while ratios greater than 10 (> 10) indicate arid conditions (Gang and Dongsheng, 2007). The relatively high Sr/Cu ratios (average 19.95 and 60.50) and low Rb/Sr ratios (average 0.27 and 0.25) of the studied sediments from the AZS and AM cores, respectively (Tables 6 and 7) indicate arid to semi-arid climate conditions. The low CIA and Rb/Sr ratios, along with the relatively high Sr/Cu ratios and elevated carbonate content of the samples (Figs. 5 and 6), indicate that these samples were deposited during arid periods and that the paleoclimate controlled the terrigenous sediment flux to the basin. These results align with the climate conditions documented by CIA, CIW, and PIA (Tables 4 and 5). Under humid climate conditions, aluminum, as a stable element held within clay minerals, remains while labile cations such as K^+ and Na^+ leach from sediments during chemical weathering (Nesbitt et al., 1980; Gao et al., 1985; Fedo et al., 1995). Therefore, high Al_2O_3/Na_2O ratios primarily reflect strong chemical weathering due to the removal of Na from parent rocks during humid climate conditions (Yang and Jung, 2004). As shown in Tables 4 and 5, the Al_2O_3/Na_2O ratios in the AZS and AM core sediments range from 4.48 to 13.47 (average 9.74) and 4.16 to 9.40 (average 6.60), respectively, indicating low chemical weathering in both core sediments. As indicated in Tables 4-7, there is a slight vertical variation in Sr/Cu, Rb/Sr, and Al_2O_3/Na_2O ratios throughout the depth profile, which is consistent with CIA, CIW, and PIA.

4.5 Recycling effect

The Index of Compositional Variability (ICV) of sediments is used as an indicator to estimate the degree of compositional maturity of the source rock (Cox et al., 1995). The

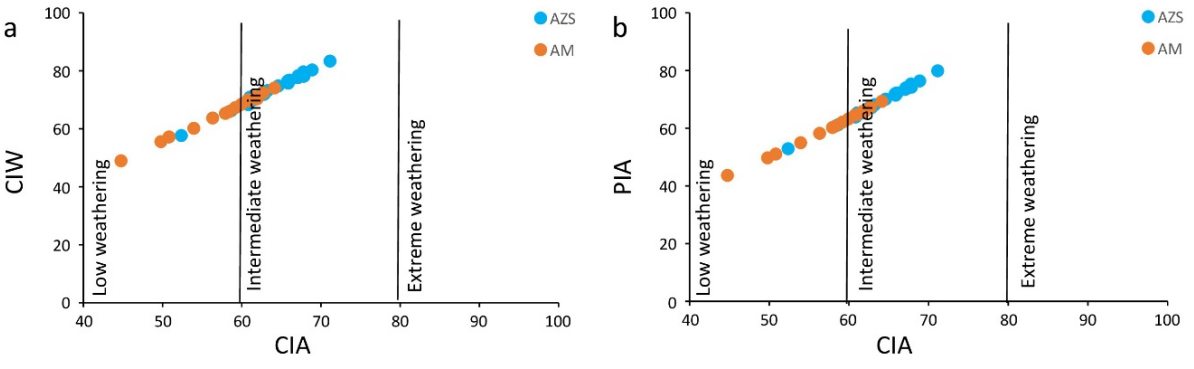

Figure 10. Binary plots of (a) CIW vs. CIA and (b) PIA vs. CIA (Shaltami, 2012) are representing paleoweathering conditions during deposition of the studied sediments. (CIA: Chemical index of alteration; PIA: Plagioclase index of alteration; CIW: Chemical index of weathering).

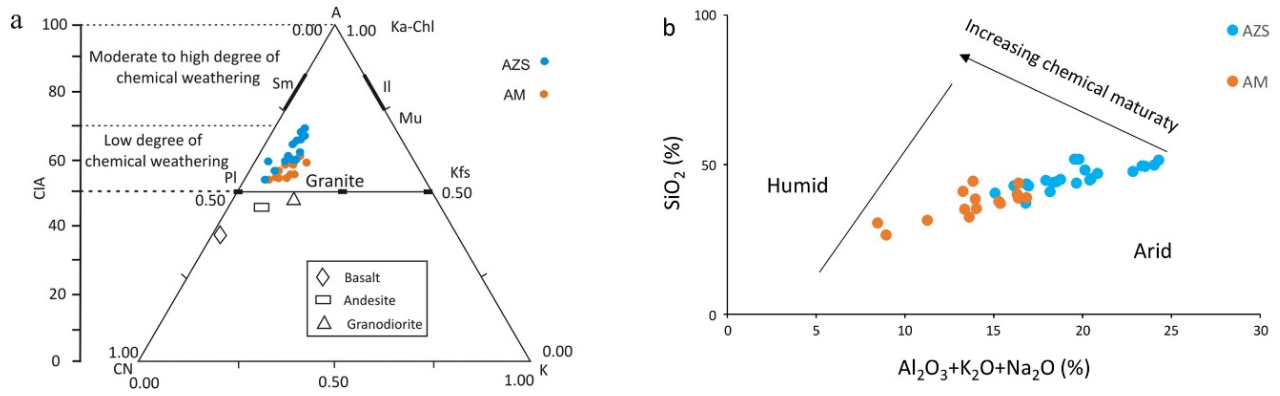

Figure 11. a) Al_2O_3-[CaO+Na_2O]-K_2O (A-CN-K; compositions as molar proportions) ternary diagram (after (Nesbitt and Young, 1982)) showing weathering trend for fine-grained sediments of AZS and AM cores, b) Bivariant major oxides plot for the studied samples according to Suttner and Dutta (1986). (kaolinite (Ka); chlorite (Chl); illite (Il); muscovite (Mu); smectite (Sm); plagioclase (Pl); K-feldspars (Kfs)).

high abundance of immature rock-forming minerals, such as plagioclase and K-feldspars (indicative of immature source rocks), as well as clay minerals like kaolinite and illite (indicative of alteration products), are associated with ICV values greater than 1 and less than 1, respectively (Cox et al., 1995). The variation in ICV values may be attributed to differences in weathering conditions and changes in source rock composition (Cox et al., 1995). To accurately determine the compositional maturity of the AZS and AM core sediments, we also examined sedimentary recycling. The ICV values of the studied samples range from 0.1 to 2.38 (average 1.57) and 0.5 to 0.62 (average 0.56) for sandy mud; 0.1 to 2.25 (average 2.21) and 0.58 to 0.76 (average 0.65) for muddy; and 0.1 to 2.91 (average 2.25) and 0.51 for silty sand facies in the AZS and AM cores, respectively (Tables 4 and 5). Overall, this suggests that the AZS core samples belong to compositionally immature rocks and can be considered as first-cycle sediments, while the AM core samples are associated with compositionally mature rocks characterized by low to moderate chemical weathering.

The vertical distributions of the geochemical indexes (CIA, CIW, PIA, and ICV) values of the two core facies from the Caspian coastal area are presented in Tables 4 and 5. The variation patterns of CIA, CIW, and PIA in the sandy mud, muddy, and silty sand facies from the AZS and AM cores are similar, whereas the trend of ICV differs from that of CIA, CIW, and PIA. The Zr/Sc ratio (Cox et al., 1995; Hassan et al., 1999) and Th/Sc ratio (McLennan et al., 1993) are useful indexes for assessing sediment recycling, compositional maturity, and intensity of alteration in source materials. Therefore, a Zr/Sc versus Th/Sc bivariate diagram was used to illustrate sorting-related fractionations in sediments. The values of Zr/Sc and Th/Sc indicate that the AZS and AM core sediments were not affected by sedimentary recycling, which is consistent with the ICV values, indicating first-cycle sedimentation during the Middle to Late Holocene (Tables 6 and 7).

4.6 Paleoredox conditions

The extent of paleo-redox states of sediments during their deposition in the basin can be evaluated through chemical analyses, such as those conducted by Dypvik (1984), Dill (1986), and Jones and Manning (1994). It is important to consider these proxies collectively, as the proxies of trace elements are not reliable when used individually. Uranium, vanadium, and nickel are combined with sediments in low capacities. Therefore, the ratios of trace elements such as U/Th, V/Cr, and Ni/Co are considered credible indicators of the depositional environment, indicating redox conditions (Tribovillard et al., 2006; Lézin et al., 2013; Zeng et al., 2015; Zhou et al., 2015; Madhava Raju et al., 2016). Under surficial conditions and weathering, U is generally oxidized and mobilized, resulting in a decrease in the U/Th ratio, indicating redox conditions (Morford et al., 2009). A U/Th ratio greater than 1.25 indicates an anoxic environment, while values ranging from 0.75 to 1.25 suggest a suboxic to a dioxic environment. A ratio of less than 0.75 indicates an oxic environment (Jones and Manning, 1994). The U/Th ratios of the sandy mud, muddy, and silty sand facies from the AZS and AM cores range from 0.34 to 0.48 (average 0.39) and 0.24 to 0.32 (average 0.29), 0.30 to 0.48 (average 0.39) and 0.16 to 0.30 (average 0.26), and 0.29 to 0.38 (average 0.32) and 0.34, respectively, indicating dysoxic to oxic conditions (Tables 6 and 7). Values of Ni/Co and V/Cr ratios greater than 7 and 4.25, respectively, indicate an anoxic environment, while values less than 5.0 and 2.0 reflect oxic environmental conditions. Jones and Manning (1994) also proposed that low to high Ni/Co values in sediments reveal oxidizing, dysoxic, and reducing conditions. The moderate values of Ni/Co ratios for the sandy mud, muddy, and silty sand facies from the AZS and AM cores range from 5.20 to 6.35 (average 5.75) and 3.94 to 5.07 (average 4.60), 5.5 to 6.58 (average 6.06) and 3.77 to 5.25 (average 4.57), and 5.9 to 6.63 (average 6.23) and 5.14, respectively, suggesting that the dominant conditions during the deposition of these deposits were dysoxic to oxic (Tables 6 and 7).

During low-oxygen conditions, V is insoluble and immobile compared to Cr, which tends to concentrate in sediments (Calvert and Pedersen, 1993; Jones and Manning, 1994). Therefore, low and high V/Cr ratios reflect oxidizing to reducing depositional conditions, respectively (Jones and Manning, 1994; Riquier et al., 2006). The V/Cr ratios of

the sandy mud, muddy, and silty sand facies from the AZS and AM cores fluctuate from 0.53 to 0.6 (average 0.56) and 0.51 to 0.57 (average 0.54), 0.4 to 0.53 (average 0.52) and 0.29 to 0.56 (average 0.42), and 0.49 to 0.54 (average 0.52) and 0.44, respectively, which are lower than the oxic threshold of 2.0, also indicating oxic conditions (Tables 6 and 7). As discussed above, the redox-sensitive trace element ratios, such as U/Th, V/Cr, and Ni/Co, indicate that the studied samples were formed under dysoxic to oxic conditions during deposition. Based on these ratios and the binary plot of Ni/Co and V/Cr against U/Th, both core samples are positioned in the dysoxic and oxic fields, displaying trends from oxic to anoxic environment (Fig. 12).

5. conclusion

Based on the XRD and geochemical analyses of fine-grained facies from the AZS and AM cores in the Jouybar and Zaghmarz areas (southern coast of the Caspian Sea), we have reached the following conclusions:

1) The bulk mineralogy of the sandy mud and muddy units in the AZS and AM cores consists of quartz, illite, mica, feldspar, and calcite minerals. The presence of abundant carbonate mineral (calcite) along with gypsum, as well as unstable components such as feldspar and rock fragments, indicates low chemical weathering conditions and arid to semi-arid climate periods during sedimentation.

2) There is a clear positive correlation between K_2O, Fe_2O_3, SiO_2, and TiO_2 with Al_2O_3 in the sediments of the AZS and AM cores, suggesting that they are hosted in clay and K-bearing minerals (particularly illite) or are derived from detrital inputs from the surrounding basin shoulders (Alborz mountains).

3) Strong to moderate positive correlations between Sc, V, and Hf with Al_2O_3 in the AZS and AM core sediments indicate their association with K-feldspar and clay minerals.

4) On the Log (Na_2O/K_2O) and Log (Fe_2O_3/K_2O) versus Log (SiO_2/Al_2O_3) plots, the most points of the studied samples lie within the shale and greywacke fields.

5) The Chemical Index of Alteration (CIA), the Chemical Index of Weathering (CIW), and the Plagioclase Index of Alteration (PIA) of both core sediments suggest semi-arid to semi-humid climatic conditions during sediment deposition, with weak to moderate chemical weathering.

6) The high Sr/Cu ratios and low Rb/Sr ratios in the studied sediments from the AZS and AM cores indicate relatively semi-arid climate conditions and the presence of carbonate rocks in the source area.

7) The index of compositional variability (ICV) of the core sediments shows negligible sedimentary recycling (compositionally immature source rocks) during transportation and deposition.

8) Overall, the redox-sensitive parameters (e.g., V/Cr, Ni/Co, U/Th) in the studied core sediments indicate dysoxic–oxic conditions in the coastal environment during the Middle to Late Holocene.

9) It is expected that the results of this study will contribute to a better understanding of the paleoclimatic conditions and paleoenvironment during the Middle to Late Holocene.

Acknowledgments

We would like to express our gratitude to the Geological Survey of Iran (GSI) for their support and assistance in data gathering, as well as for granting permission to publish this paper. We also extend our thanks to the staff of the Sediment Group for their valuable field assistance.

Authors contributions

Authors have contributed equally in preparing and writing the manuscript.

Availability of data and materials

The data that support the findings of this study are available from the corresponding author, upon reasonable request.

Conflict of interests

The authors declare that they have no known competing financial interests or personal relationships that could have appeared to influence the work reported in this paper.

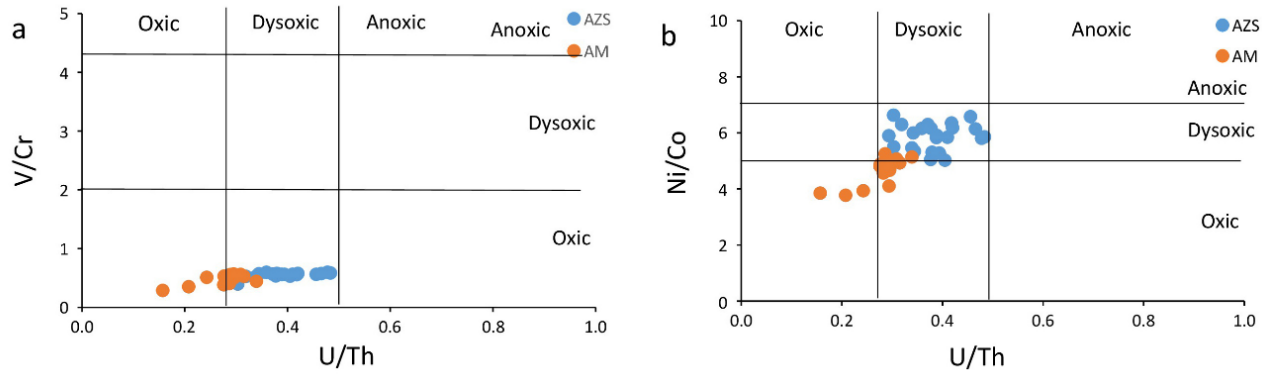

Figure 12. Binary plots of some trace element ratios used as proxies to infer palaeoredox conditions during the deposition of the AZS and AM core sediments, a) V/Cr vs. U/Th, and b) Ni/Co vs. U/Th (Wang et al., 2017).

References

Aghanabati A. (2004) Geology of Iran. *Geological Survey and mineral exploration of Iran,* In Persian

Al-Khirbash S., Al-Semhi K., Richard L., Nasir S., Al-Harthy A. R. (2013) Rare earth element mobility during laterization of the mafic rocks of the Oman Mountains. *Arabian Journal of Geosciences* 7:5443–5454. DOI: https://doi.org/10.57647/j.ijes.2025.16794.

Armstrong-Altrin J. S., Lee Y. I., Verma S. P., Ramasamy S. (2004) Geochemistry of sandstones from the upper Miocene Kudankulam Formation Southern India: implications for provenance, weathering and tectonic setting. *Journal of sedimentary Research* 74 (2): 285–297. DOI: https://doi.org/10.1306/082803740285.

Bai Y., Liu Z., Sun P., Liu R., Hu X., Zhao H., Xu Y. (2015) Rare earth and major element geochemistry of Eocene fine-grained sediments in oil shale- and coal-bearing layers of the Meihe Basin, northeast China.. *Journal of Asian Earth Sciences* 97:89–101. DOI: https://doi.org/10.1016/j.jseaes.2014.10.008.

Bauluz B., Mayayo M. J., Fernandez-Nieto C., Gonzalez Lopez J. M. (2000) Geochemistry of Precambrian and Paleozoic siliciclastic rocks from the Iberian Range (NE Spain): implications for source-area weathering, sorting, provenance, and tectonic setting. *Chemical Geology* 168 (1-2): 135–150. DOI: https://doi.org/10.1016/S0009-2541(00)00192-3.

Bhatia M. R., Crook K. A. (1986) Trace element characteristics of greywackes and tectonic setting discrimination of sedimentary basins. *Contributions to Mineralogy and Petrology* 92 (2): 181–193. DOI: https://doi.org/10.1007/BF00375292.

Calvert S. E., Pedersen T. F. (1993) Geochemistry of recent oxic and anoxic sediments: implications for the geological record. *Marine geology* 113 (1-2): 67–88. DOI: https://doi.org/10.1016/0025-3227(93)90150-T.

Campo M. D., Papa C. D., Jiménez-Millán J., Nieto F. (2007) Clay mineral assemblages and analcime formation in a Palaeogene fluvial-lacustrine sequence (Maíz Gordo Formation Palaeogen) from northwestern Argentina. *Sedimentary Geology* 201 (1-2): 56–74. DOI: https://doi.org/10.1016/j.sedgeo.2007.04.007.

Cao H. S., Guo W., Shan X. L., Ma L., Sun P. C. (2015) Paleolimnological environments and organic accumulation of the Nenjiang Formation in the Southeastern Songliao Basin, China. *Oil Shale* 32 (1): 5–24. DOI: https://doi.org/10.3176.

Cardenas A., Girty G. H., Hanson A. D., Lahren M. M. (1996) Assessing differences in composition between low metamorphic grade mudstone and high-grade schists using log ratio techniques. *The Journal of Geology* 104:279–293. DOI: https://doi.org/10.1086/629825.

Chamley H. (1989) Clay Minerals. In: Clay Sedimentology. *Springer,* 3–20.

Chen J., An Z., Liu L., Ji J., Yang J., Chen Y. (2001) Variations in chemical compositions of the eolian dust in Chinese Loess Plateau over the past 2.5 Ma and chemical weathering in the Asian inland. *Science in China Series D: Earth Science* 44:403–413. DOI: https://doi.org/10.1007/BF02909779.

Christopher R. G., Elderfield H. (1990) Application of the Ce anomaly as a paleoredox indicator: the ground rules. *Paleoceanography* 5:823–833. DOI: https://doi.org/10.1029/PA005i005p00823.

Cingolani C. A., Manassero M., Abre P. (2003) Composition, provenance, and tectonic setting of Ordovician siliciclastic rocks in the San Rafael block: Southern extension of the Precordillera crustal fragment, Argentina. *Journal of South American Earth Sciences* 16:91–106. DOI: https://doi.org/10.1016/S0895-9811(03)00021-X.

Cox R., Lowe D. R., Cullers R. L. (1995) The influence of sediment recycling and basement composition on evolution of mud rock chemistry in the southwestern United States. *Geochimica et Cosmochimica Acta* 59:2919–2940. DOI: https://doi.org/10.1016/0016-7037(95)00185-9.

Cullers R. L. (1988) Mineralogical and chemical changes of soil and stream sediment formed by intense weathering of the Danburg granite, Georgia, U.S.A. *Lithos* 21:301–314. DOI: https://doi.org/10.1016/0024-4937(88)90035-7.

——— (2000) The geochemistry of shales, siltstones and sandstones of Pennsylvanian-Permian age, Colorado, USA: Implications for provenance and metamorphic studies. *Lithos* 51:181–203. DOI: https://doi.org/10.1016/S0024-4937(99)00063-8.

Cullers R. L., Podkovyrov V. N. (2000) Geochemistry of the Mesoproterozoic Lakhanda shales in southeastern Yakutia, Russia: Implications for mineralogical and provenance control, and recycling. *Precambrian Research* 104:77–93. DOI: https://doi.org/10.1016/S0301-9268(00)00090-5.

Das B. K., Al-Mikhlafi A. S., Kaur P. (2006) Geochemistry of Mansar Lake sediments, Jammu, India: Implication for Source-area weathering, provenance, and tectonic setting. *Journal of Asian Earth Sciences* 26:649–668. DOI: https://doi.org/10.1016/j.jseaes.2005.01.005.

Deepthi K., Natesan U., Muthulakshmi A. L., Ferrer V. A., Venugopalan V. P., Narasimhan S. V. (2013) Geochemical characteristics and depositional environment of Kalpakkam, southeast coast of India. *Environmental earth sciences* 69:2357–2364. DOI: https://doi.org/10.1007/s12665-012-2065-5.

Dill H. (1986) Metallogenesis of Early Paleozoic Graptolite Shales from the Graefenthal Horst (Northern Bavaria-Federal Republic of Germany). *Economic Geology* 81:889–903. DOI: https://doi.org/10.2113/gsecongeo.81.4.889.

Dixon J. B., Weed S. B. (1992) Minerals in soil environments. *Soil Science Society of America Journal*

Dypvik H. (1984) Geochemical compositions and depositional conditions of Upper Jurassic and Lower Cretaceous Yorkshire clays.England. *Geological Magazine* 121:489–504. DOI: https://doi.org/10.1017/S0016756800030028.

Fedo C. M., Eriksson K. A., Krogstad E. J. (1996) Geochemistry of shales from the Archean (3.0 Ga) Buhwa Greenstone Belt, Zimbabwe: implications for provenance and source area weathering. *Geochimica et Cosmochimica Acta* 60:1751–1763. DOI: https://doi.org/10.1016/0016-7037(96)00058-0.

Fedo C. M., Nesbitt H. W., Young G. M. (1995) Unravelling the effects of potassium metasomatism in sedimentary rocks and paleosols, with implications for paleoweathering conditions and provenance. *Geology* 23:921–924. DOI: https://doi.org/10.1130/0091-7613(1995)023$¡$0921:UTEOPM$¿$2.3.CO;2.

Fedo C. M., Young G. M., Nesbitt G. M. (1997a) Paleoclimatic control on the composition of the Paleoproterozoic serpent formation, Huronian supergroup, Canada: a green-house to icehouse transition. *Precambrian Research* 86:201–223.

Fedo C. M., Young G. M., Nesbitt H. W., Hanchar J. M. (1997b) Potassic and sodic metasomatism in the southern Province of the Canadian Shield: evidence from the Paleoproterozoic serpent formation, Huronian supergroup, Canada. *Precambrian Research* 84:17–36. DOI: https://doi.org/10.1016/S0301-9268(96)00058-7.

Folk R. L. (1974) Petrography of Sedimentary Rocks. *Hemphill Publishing Company,* 182.

Fu X. G., Wang J., Chen W. B., Feng X. L., Wang D., Song C. Y., Zeng S. Q. (2016) Elemental geochemistry of the early Jurassic black shales in the Qiangtang Basin, eastern Tethys: constraints for paleoenvironment conditions. *Geological Journal* 51:443–454.

——— (2015) Organic accumulation in lacustrine rift basin: constraints from mineralogical and multiple geochemical proxies. *International Journal of Earth Sciences* 104:495–511.

Fu X. G., Wang J., Zeng Y. H., Tan F. W., He J. L. (2011) Geochemistry and origin of rare earth elements (REEs) in the Shengli River oil shale, northern Tibet, China. *Geochemistry* 71:21–30.

Gallala W., Gaied M. E., Montacer M. (2009) Detrital mode, mineralogy and geochemistry of the Sidi Aïch Formation (Early Cretaceous) in central and southwestern Tunisia: Implications for provenance, tectonic setting and paleoenvironment. *Journal of African Earth Sciences* 53:159–170. DOI: https://doi.org/10.1016/j.jafrearsci.2009.01.002.

Gang L., Dongsheng Z. (2007) Application of microelements analysis in identifying sedimentary environment-taking Qianjiang Formation in the Jianghan Basin as an example. *Petroleum Geology & Experimental* 29:307–310. DOI: https://doi.org/10.11781/sysydz200703307.

Gao S., Dong G., Li B. (1985) The variable of chemical elements contents in paleo-Aeolian sand strata and climatic environment at Yulin area, Shaanxi province. *Journal of desert research* 5:25–30.

Ghosh S., Sarkar S., Ghosh P. (2012) Petrography and major element geochemistry of the Permo Triassic sandstones, central India: implications for provenance in an intracratonic pull-apart basin. *Journal of Asian Earth Sciences* 43:207–240. DOI: https://doi.org/10.1016/j.jseaes.2011.09.011.

Gosse J. C., Fred M. P. (2001) Terrestrial in situ cosmogenic nuclides: theory and application. *Quaternary Science Reviews* 20:1475–1560.

Gromet L. P., Dymek R. F., Haskin L. A., Korotev R. V. (1984) The North American shale composite: its composition, major and trace element characteristics. *Geochimica et Cosmochimica Acta* 48:2469–2482. DOI: https://doi.org/https://doi.org/10.1016/0016-7037(84)90298-9.

Harnois L. (1988) The new index, a new chemical index of weathering. *Sedimentary geology* 55:319–322. DOI: https://doi.org/10.1016/0037-0738(88)90137-6.

Hassan S., Ishiga H., Roser B. P., Dozen K., Naka T. (1999) Geochemistry of Permian Triassic shales in the Salt range, Pakistan: implications for provenance and tectonism at the Gondwana margin. *Chemical Geology* 158:293–314. DOI: https://doi.org/10.1016/S0899-5362(99)90065-9.

Herron M. M. (1988) Geochemical classification of terrigenous sands and shales from core of log data. *Journal of Sedimentary Research* 58:820–829. DOI: https://doi.org/10.1306/212F8E77-2B24-11D7-8648000102C1865D.

Hessler A. M., Lowe D. R. (2006) Weathering and sediment generation in the Archean: an integrated study of the evolution of siliciclastic sedimentary rocks of the 3.2 Ga Moodies Group, Barberton Greenstone Belt, South Africa. *Precambrian Research* 151:185–210. DOI: https://doi.org/10.1016/j.precamres.2006.08.008.

Jin Z., Li F., Cao J., Wang S., Yu J. (2006) Geochemistry of Daihai lake sediments, Inner Mongolia, north China: Implications for provenance, sedimentary sorting, and catchment weathering. *Geomorphology* 80:147–163. DOI: https://doi.org/10.1016/j.geomorph.2006.02.006.

Jin Z. D., Zhang E. L. (2002) Paleoclimate implication of Rb/Sr ratios from lake sediments. *Science and Technology Engineering* 2:20–22.

Jones B., Manning D. A. (1994) Comparison of geochemical indices used for the interpretation of paleo-redox conditions in ancient mudstones. *Chemical geology* 111:111–129. DOI: https://doi.org/10.1016/0009-2541(94)90085-X.

Lahijani H., Tavakoli V. (2012) Identifying provenance of South Caspian coastal sediments using mineral distribution pattern. *Quaternary International* 261:128–137. DOI: https://doi.org/10.1016/j.quaint.2011.04.021.

Lee Y. I. (2009) Geochemistry of shales of the Upper Cretaceous Hayang Group, SE Korea: Implications for provenance and source weathering at an active continental margin Sediment. *Sedimentary Geology* 215:1–12. DOI: https://doi.org/10.1016/j.sedgeo.2008.12.004.

Lerman A., Imboden D. M., Gat J. R. (1995) Physics and chemistry of lakes. *Springer-Verlag, Berlin*

Li Y., Wang N., Cheng H. Y., Long H., Zhao Q. (2009) Holocene environmental change in the marginal area of the Asian monsoon: a record from Zhuye Lake, NW China. *Boreas* 38:349–361. DOI: https://doi.org/10.1111/j.1502-3885.2008.00063.x.

Lézin C., Andreu B., Pellenard P., Bouchez J. L., Emmanuel L., Fauré P., Landrein P. (2013) Geochemical disturbance and paleoenvironmental changes during the Early Toarcian in NW Europe. *Chemical Geology* 341:1–15. DOI: https://doi.org/10.1016/j.chemgeo.2013.01.003.

Ma P. F., Wang L. C., Wang C. S., Wu X. H., Wei Y. S. (2015) Organic-matter accumulation of the lacustrine lunpola oil shale, central Tibetan plateau: controlled by the paleoclimate, provenance, and drainage system. *International Journal of Coal Geology* 147:58–70. DOI: https://doi.org/10.1016/j.coal.2015.06.011.

Madhava Raju J., Ramírez-Montoya E., Monreal R., González-León C. M., Pi-Puig T., Espinoza-Maldonado I. G., Grijalva-Noriega F. J. (2016) Paleoclimate, paleoweathering and paleoredox conditions of Lower Cretaceous shales from the Mural Limestone, Tuape section, northern Sonora, Mexico: constraints from clay mineralogy and geochemistry. *Revista Mexicana de Ciencias Geológicas* 33:34–48.

Mazumder R. (2017) Sediment provenance, Influences on compositional change from source to sink. *Sediment Provenance,* DOI: https://doi.org/10.1016/B978-0-12-803386-9.00001-0.

McLennan S. M., Hemming S., McDaniel D. K., Hanson G. N. (1993) Geochemical approaches to sedimentation, provenance, and tectonics. *Special Papers-Geological Society of America* 21 DOI: https://doi.org/10.1130/SPE284-p21.

McLennan S. M., Taylor S. R., Kröner A. (1983) Geochemical evolution of Archean shales from South Africa, The Swaziland and Pongola Supergroups. *Precambrian Research* 22:93–124. DOI: https://doi.org/10.1016/0301-9268(83)90060-8.

Meng Q. T., Liu Z. J., Bruch A. A. (2012) Paleoclimatic evolution during the Eocene and its influence on oil shale mineralization, Fushun Basin, China. *Journal of Asian Earth Sciences* 45:95–105. DOI: https://doi.org/10.1016/j.jseae s.2011.09.021.

Moradi A. V., Sari A., Akkaya P. (2016) Geochemistry of the Miocene oil shale (Hançili Formation) in the Çankırı-Çorum Basin, Central Turkey: implications for Paleoclimate conditions, source-area weathering, provenance and tectonic setting. *Sedimentary Geology* 341:289–303.

Morford J. L., Martin W. R., Carney C. M. (2009) Uranium diagenesis in sediments underlying bottom waters with high oxygen content. *Geochimica et Cosmochimica Acta* 73:2920–2937. DOI: https://doi.org/10.1016/j.gca.2009.02.014.

Nath B. N., Bau M., Rao B. R., Rao C. M. (1997) Trace and rare earth elemental variation in Arabian Sea sediments through a transect across the oxygen smallest zone. *Geochimica et Cosmochimica Acta* 61:2375–2388. http://drs.nio.org/drs/handle/2264/2004

Nesbitt H. W., Markovics G., Price R. C. (1980) Chemical processes affecting alkalis and alkaline earth during continental weathering. *Geochimica et cosmochimica acta* 44:1659–1666. DOI: https://doi.org/10.1016/0016-7037(80)90218-5.

Nesbitt H. W., Young G. M. (1982) Early Proterozoic climates and plate motions inferred from major element chemistry of lutites. *Nature* 299:15–717. DOI: https://doi.org/10.1038/299715a0.

——— (1984) Prediction of some weathering trends of plutonic and volcanic rocks based on thermodynamic and kinetic considerations. *Geochimica et cosmochimica acta* 48:1523–1534. DOI: https://doi.org/10.1016/0016-7037(84)90408-3.

Pettijohn F. J., Potter P. E., Siever R. (2012) Sand and sandstone. *Springer Science & Business Media,* DOI: https://doi.org/10.1007/978-1-4612-1066-5.

Rahman M. J. J., Suzuki S. (2007) Composition of Neogene shales from the Surma Group, Bengal Basin, Bangladesh: Implications for provenance and tectonic setting. *Austrian Journal of Earth Sciences* 100:54–104.

Riquier L., Tribovillard N., Averbuch O., Devleeschouwer X., Riboulau A. (2006) The Late Frasnian Kellwasser horizons of the Harz Mountains (Germany): two oxygen-deficient periods resulting from different mechanism. *Chemical Geology* 233:137–155. DOI: https://doi.org/10.1016/j.chemgeo.2006.02.021.

Roy D., Roser B. P. (2012) Geochemistry of the Tertiary sequence in the Shahbajpur-1 well, Hatia Trough, Bengal Basin, Bangladesh: Provenance, source weathering and province affinity. *Journal of Life and Earth Science* 7:1–13. DOI: https://doi.org/10.3329/jles.v7i0.20115.

Sahoo P. K., Guimaraes J. T. F., Souza-Filho P. W. M., Da Silvam M. S., Maturity C. W., Powell M. A. (2016) Geochemistry of upland lacustrine sediments from Serra dos Carajas, Southeastern Amazon, Brazil: Implications for catchment weathering, provenance, and sedimentary processes. *Journal of South American Earth Sciences* 72:178–190. DOI: https://doi.org/10.1016/j.jsames.2016.09.003.

Selvaraj K., Chen C. T. A. (2006) Moderate chemical weathering of subtropical Taiwan: constraints from solid-phase geochemistry of sediments and sedimentary rocks. *The Journal of Geology* 114:101–116. DOI: https://doi.org/10.1086/498102.

Shaltami O. R. (2012) Mineral composition and environmental geochemistry of the beach sediments along the Mediterranean coast from Benghazi to Bin Jawwad, Northeast Libya. 139

Song Y., Liu Z., Meng Q., Wang Y. (2016) Petrography and geochemistry characteristics of the lower Cretaceous Muling Formation from the Laoheishan Basin, Northeast China: implications for provenance and tectonic setting. *Mineralogy and Petrology* 111:383–397.

Sun L. H., Gui H. R., Chen S. (2012) Geochemistry of sandstones from the Neoproterozoic Shijia Formation, northern Anhui Province, China: implications for provenance, weathering and tectonic setting. *Geochemistry* 72:253–260. DOI: https://doi.org/10.1016/j.chemer.2011.11.006.

Suttner L. J., Dutta P. K. (1986) Alluvial sandstone composition and paleoclimate; I, Framework mineralogy. *Journal of Sedimentary Research* 56:329–345. DOI: https://doi.org/10.1306/212F8909-2B24-11D7-8648000102C1865D.

Tao H. F., Sun S., Wang Z. Q., Yang X. F., Jiang L. (2014) Petrography and geochemistry of Lower Carboniferous greywacke and mudstones in Northeast Junggar, China: implications for provenance, source weathering, and tectonic setting. *Journal of Asian Earth Sciences* 87:11–25. DOI: https://doi.org/10.1016/j.jseaes.2014.02.007.

Taylor S. R., McLennan S. M. (1985) The Continental Crust: Its Composition and Evolution. *Blackwell Scientific Publications,* DOI: https://doi.org/10.1017/S0016756800032167.

Tribovillard N., Algeo T. J., Lyons T., Riboulleau A. (2006) Trace metals as paleoredox and paleoproductivity proxies: an update. *Chemical geology* 232:12–32. DOI: https://doi.org/10.1016/j.chemgeo.2006.02.012.

Vahdati Daneshmand F., Saidi A. (1991) Explanatory text of the Sari quadrangle map, Iran, Scale 1:250000. *Geological Survey and mineral exploration of Iran,* In Persian

Verma S. P., Armstrong-Altrin J. S. (2013) New multi-dimensional diagrams for tectonic discrimination of siliciclastic sediments and their application to Precambrian basins. *Chemical Geology* 355:117–133. DOI: https://doi.org/10.1016/j.chemgeo.2013.07.014.

Von Eynatten H., Barceló-Vidal C., Pawlowsky-Glahn V. (2003) Modelling compositional change: the example of chemical weathering of granitoid rocks. *Mathematical Geology* 35:231–251. DOI: https://doi.org/10.1023/A:1023835513705.

Wang Z. W., Wang J., Fu X. G., Zhan W. Z., Yu F., Feng X. L., Song C. Y., Chen W. B., Zeng S. Q. (2017) Organic material accumulation of Carnian mudstones in the North Qiantang Depression, eastern Tethys: controlled by the paleoclimate, paleoenvironment, and provenance. *Marine and Petroleum Geology* 88:440–457.

Wei Z. Q., Zhong W., Chen Y. Q., Tan L. L. (2015) Supergene geochemical elements of swampy basin in the sub-tropical monsoon region: a case study of Dingnan Dahu in Jiangxi Province. *Progress in Geography* 34:909–917. DOI: https://doi.org/10.18306/dlkxjz.2015.07.012.

Wilmsen M., Fürsich F. T., Seyed-Emami K., Majidifard M. R., Taheri J. (2009) The Cimmerian Orogeny in northern Iran: tectono-stratigraphic evidence from the foreland. *Terra Nova* 21:211–218. DOI: https://doi.org/10.1111/j.1365-3121.2009.00876.x.

Yan D. T., Chen D. Z., Wang Q. C., Wang J. G. (2010) Large-scale climate fluctuations in the latest Ordovician on the Yangtze block, South China. *Geology* 38:599–602. DOI: https://doi.org/10.1130/G30961.1.

Yang S., Jung H. S. (2004) Two unique weathering regimes in the Changjiang and Huanghe drainage basins: geochemical evidence from river sediments. *Sedimentary Geology* 164:19–34. DOI: https://doi.org/10.1016/j.sedgeo.2003.08.001.

Yunfei W. (1993) Lacustrine carbonate chemical sedimentation and climatic-environmental evolution-a case study of Qinghai lake and Daihai lake. *Oceanologia et Limnologia Sinica* 24:31–36.

Zeng S. Q., Wang J., Fu X. G., Chen W. B., Feng X. L., Wang D., Song C. Y., Wang Z. W. (2015) Geochemical characteristics, redox conditions, and organic matter accumulation of marine oil shale from the Chang liang Mountain area, northern Tibet. China. *Marine and Petroleum Geology* 64:203–221. DOI: https://doi.org/10.1016/j.marpetgeo.2015.02.031.

Zhang L. F., Sun M., Wang S. G., Yu X. Y. (1998) The composition of shales from the Ordos basin, China: effects of source weathering and diagenesis. *Sedimentary Geology* 116:129–141. DOI: https://doi.org/10.1016/S0037-0738(97)00074-2.

Zhou L., Algeo T. J., Shen J., Hu Z. F., Gong H., Xie S., Huang J. H., Gao S. (2015) Changes in marine productivity and redox conditions during the late Ordovician Hirnantian glaciation. *Paleogeography. Palaeoclimatology. Paleoecology* 420:223–234. DOI: https://doi.org/10.1016/j.palaeo.2014.12.012.